ECORFAN®

ECORFAN-Democratic Republic of Congo

Definition of Journal

Scientific Objectives

Support the international scientific community in its written production Science, Technology and Innovation in the Field of Physical Sciences Mathematics and Earth sciences, in Subdisciplines of image and signal processing, control-digital system-artificial, intelligence-fuzzy, logic-mathematical, modeling-computational, mathematics-computer, science.

ECORFAN-Mexico SC is a Scientific and Technological Company in contribution to the Human Resource training focused on the continuity in the critical analysis of International Research and is attached to CONACYT-RENIECYT number 1702902, its commitment is to disseminate research and contributions of the International Scientific Community, academic institutions, agencies and entities of the public and private sectors and contribute to the linking of researchers who carry out scientific activities, technological developments and training of specialized human resources with governments, companies and social organizations.

Encourage the interlocution of the International Scientific Community with other Study Centers in Mexico and abroad and promote a wide incorporation of academics, specialists and researchers to the publication in Science Structures of Autonomous Universities - State Public Universities - Federal IES - Polytechnic Universities - Technological Universities - Federal Technological Institutes - Normal Schools - Decentralized Technological Institutes - Intercultural Universities - S & T Councils - CONACYT Research Centers.

Scope, Coverage and Audience

ECORFAN-Democratic Republic of Congo is a Journal edited by ECORFAN-Mexico S.C in its Holding with repository in Democratic Republic of Congo, is a scientific publication arbitrated and indexed with semester periods. It supports a wide range of contents that are evaluated by academic peers by the Double-Blind method, around subjects related to the theory and practice of image and signal processing, control-digital system-artificial, intelligence-fuzzy, logic-mathematical, modeling-computational, mathematics-computer, science with diverse approaches and perspectives , That contribute to the diffusion of the development of Science Technology and Innovation that allow the arguments related to the decision making and influence in the formulation of international policies in the Field of Physical Sciences Mathematics and Earth sciences. The editorial horizon of ECORFAN-Mexico® extends beyond the academy and integrates other segments of research and analysis outside the scope, as long as they meet the requirements of rigorous argumentative and scientific, as well as addressing issues of general and current interest of the International Scientific Society.

Arbitration Committee

IBARRA-MANZANO, Oscar Gerardo. PhD
Instituto Nacional de Astrofísica, Óptica y Electrónica

JIMÉNEZ - GARCÍA, José Alfredo. PhD
Centro de Innovación Aplicada en Tecnologías Competitivas

GARCÍA - RODRÍGUEZ, Martha Leticia. PhD
Centro de Investigaciones y de Estudios Avanzados

PANTOJA - RANGEL, Rafael. PhD
Universidad de Guadalajara

PARADA - RICO, Sandra Evely. PhD
Centro de Investigación y Estudios Avanzados

REYES - RODRÍGUEZ, Aarón Víctor. PhD
Centro de Investigación y Estudios Avanzados

ZALDÍVAR - ROJAS, José David. PhD
Centro de Investigación y Estudios Avanzados

VÁZQUEZ-LÓPEZ, José Antonio. PhD
Tecnológico Nacional de México en Celaya

GARCÍA - TORRES, Erika. PhD
Centro de Investigación y de Estudios Avanzados del Instituto Politécnico Nacional

PÁEZ, David Alfonso. PhD
Centro de Investigación y de Estudios Avanzados del Instituto Politécnico Nacional

OLVERA - MARTÍNEZ, María del Carmen. PhD
Centro de Investigación y de Estudios Avanzados del Instituto Politécnico Nacional

Assignment of Rights

The sending of an Article to ECORFAN-Democratic Republic of Congo emanates the commitment of the author not to submit it simultaneously to the consideration of other series publications for it must complement the Originality Format for its Article.

The authors sign the Authorization Format for their Article to be disseminated by means that ECORFAN-Mexico, S.C. In its Holding Democratic Republic of Congo considers pertinent for disclosure and diffusion of its Article its Rights of Work.

Declaration of Authorship

Indicate the Name of Author and Coauthors at most in the participation of the Article and indicate in extensive the Institutional Affiliation indicating the Department.

Identify the Name of Author and Coauthors at most with the CVU Scholarship Number-PNPC or SNI-CONACYT- Indicating the Researcher Level and their Google Scholar Profile to verify their Citation Level and H index.

Identify the Name of Author and Coauthors at most in the Science and Technology Profiles widely accepted by the International Scientific Community ORC ID - Researcher ID Thomson - arXiv Author ID - PubMed Author ID - Open ID respectively.

Indicate the contact for correspondence to the Author (Mail and Telephone) and indicate the Researcher who contributes as the first Author of the Article.

Plagiarism Detection

All Articles will be tested by plagiarism software PLAGSCAN if a plagiarism level is detected Positive will not be sent to arbitration and will be rescinded of the reception of the Article notifying the Authors responsible, claiming that academic plagiarism is criminalized in the Penal Code.

Arbitration Process

All Articles will be evaluated by academic peers by the Double Blind method, the Arbitration Approval is a requirement for the Editorial Board to make a final decision that will be final in all cases. MARVID® is a derivative brand of ECORFAN® specialized in providing the expert evaluators all of them with Doctorate degree and distinction of International Researchers in the respective Councils of Science and Technology the counterpart of CONACYT for the chapters of America-Europe-Asia-Africa and Oceania. The identification of the authorship should only appear on a first removable page, in order to ensure that the Arbitration process is anonymous and covers the following stages: Identification of the Journal with its author occupation rate - Identification of Authors and Coauthors - Detection of plagiarism PLAGSCAN - Review of Formats of Authorization and Originality-Allocation to the Editorial Board- Allocation of the pair of Expert Arbitrators-Notification of Arbitration - Declaration of observations to the Author-Verification of Article Modified for Editing-Publication.

Instructions for Scientific, Technological and Innovation Publication

Knowledge Area

The works must be unpublished and refer to topics of Image and signal processing, control-digital system-artificial, intelligence-fuzzy, logic-mathematical, modeling-computational, mathematics-computer, science and other topics related to Physical Sciences Mathematics and Earth sciences.

Presentation of the Content

In the first article we present, *Development of an artificial neural network for the prediction of the thermodynamic property enthalpy in the NH₃-H₂O mixture*, by VERA-ROMERO, Iván, PEREZ-AVIÑA, L. Fernando, MÉNDEZ-ÁBREGO, V. Manuel and MARTÍNEZ-REYES, José, with adscription in the Universidad de la Ciénega del Estado de Michoacán de Ocampo, as the next article we present, *Rotor crack moment of inertia*, by JIMÉNEZ RABIELA, Homero, VÁZQUEZ GONZÁLEZ, Benjamín, RAMÍREZ CRUZ, José Luis e ILIZALITURRI BADILLO, Joshua Suraj, with adscription in the Universidad Autónoma Metropolitana, as the next article we present, *Analysis of the use of aerogel as a thermal insulator in refrigerated containers for storing blood using a photovoltaic system*, by VALLE-HERNANDEZ, Julio, MANZANO-MUÑOZ, Meily Yoselin, ROMÁN-AGUILAR, Raúl and DELGADILLO-AVILA, Wendy Montserrath, with adscription in the Universidad Autónoma del Estado de Hidalgo, as the last article we present, *Design and 3D printing of the Robot, articulated with 6 degrees of freedom with educational applications*, by SÁNCHEZ-GUARNEROS, Raziel, MARTÍNEZ-HERNÁNDEZ, Haydee Patricia, CORTES-MALDONADO, Raúl and BEDOLLA-HERNÁNDEZ, Jorge, with adscription in the Instituto Tecnológico de Apizaco.

Content

Article   Page

Development of an artificial neural network for the prediction of the thermodynamic property enthalpy in the NH₃-H₂O mixture

Implementación de una red neuronal artificial para la predicción de la propiedad termodinámica entalpia en la mezcla NH₃-H₂O

VERA-ROMERO, Iván†*, PEREZ-AVIÑA, L. Fernando, MÉNDEZ-ÁBREGO, V. Manuel and MARTÍNEZ-REYES, José

Universidad de la Ciénega del Estado de Michoacán de Ocampo, México.

ID 1ˢᵗ Author: *Iván, Vera-Romero* / **ORC ID:** 0000-0003-1771-6630, **CVU CONACYT ID:** 102272

ID 1ˢᵗ Co-author: *L. Fernando, Perez-Aviña*

ID 2ⁿᵈ Co-author: *V. Manuel, Méndez-Ábrego* / **ORC ID:** 0000-0003-3409-8619, **CVU CONACYT ID:** 596022

ID 3ʳᵈ Co-author: *José, Martínez-Reyes* / **ORC ID:** 0000-0001-6601-1851, **CVU CONACYT ID:** 232124

Abstract

There are many different methodologies for calculating the enthalpy thermodynamic property in the ammonia-water mixture, which is mainly used in the analysis of absorption refrigeration systems and power, so its prediction becomes essential not only for theoretical evaluations, also for the design of industrial equipment. In this work an alternative methodology, an artificial neural network (ARN) is approached. Two neural networks were designed: ARN A and ARN B. ARN A has three main input variables: Pressure (P), Temperature (T) and Ammonia Concentration in the mixture (x), to obtain the output variable: enthalpy. ARN B has as a particular case that the variable Temperature (T) is replaced by the phase in which the mixture is found (q); both networks were compared with experimental data reported in open literature and with the EES™ software. The two networks are capable of predicting the enthalpy of the Ammonia-Water mixture, ARN A with an acceptable prediction range between 100 kPa and 11,000 kPa, and ARN B from 5,000 kPa to 10,000 kPa.

Ammonia-water, Artificial neural network, Enthalpy

Resumen

Existen diferentes metodologías para el cálculo de la propiedad termodinámica Entalpia en la mezcla amoniaco-agua, la cual es principalmente empleada en el análisis de sistemas de refrigeración por absorción y de potencia, por lo que su predicción se vuelve indispensable no solo para las evaluaciones teóricas sino también para el diseño de equipos industriales. En este trabajo se aborda una metodología alternativa, una red neuronal artificial (RNA). Se diseñaron dos redes neuronales: Red A y Red B. La Red A cuenta con tres variables principales de entrada: Presión (P), Temperatura (T) y Concentración de Amoniaco en la mezcla (x), para obtener la variable de salida: Entalpia. La Red B, tiene como caso particular que se sustituye la variable Temperatura (T) por la fase en la que se encuentra la mezcla (q); ambas redes fueron comparadas con datos experimentales reportados en literatura abierta y con el software EES™. Las dos redes son capaces de predecir la entalpia de la mezcla Amoniaco-Agua, la Red A con un rango de predicción aceptable entre 100 kPa y 11,000 kPa, y la Red B de 5,000 kPa a 10,000 kPa.

Amoniaco-agua, Red neuronal artificial, Entalpia

Citation: VERA-ROMERO, Iván, PEREZ-AVIÑA, L. Fernando, MÉNDEZ-ÁBREGO, V. Manuel and MARTÍNEZ-REYES, José. Development of an artificial neural network for the prediction of the thermodynamic property enthalpy in the NH3-H2O mixture. ECORFAN Journal-Democratic Republic of Congo. 2022. 8-15:1-10.

---

* Author's Correspondence (ivera@ucemich.edu.mx)
† Researcher contributing first author.

Introduction

The thermodynamic properties of the ammonia-water mixture are widely used in the design and simulation of absorption refrigeration equipment, flow extraction, power equipment, among others (Kalina, 1983; Stecco & Desideri, 1989). Mainly, the enthalpy property is used to perform energy balances (Tillner-Roth & Friend, 1998b), it is for this reason that having a reliable methodology is of utmost importance for obtaining this property (Thorin, 2001; Thorin et al., 1998).

There are different solution methodologies for the calculation of thermodynamic properties for the ammonia-water mixture (Tillner-Roth & Friend, 1998a), which can be mainly divided into 7 groups, which are (Thorin, 2000): cubic equation of state, Gibbs energy of Excess, law of corresponding states, group contribution method, polynomial functions and viral equation of state, therefore the possibility of an eighth methodology is detected which corresponds to that of constructing an artificial neural network (ANN) and which so far has not been widely explored as a prediction possibility (Vera-Romero & Heard-Wade, 2017b).

Some mathematical models have been programmed in software such as the Engineering Equation Solver (EES™) and the REFPROP™ of the National Institute of Standards and Technology (NIST) because of their certainty and range of application; however, these softwares are commercial. The latter work with different methodologies, EES uses the methodology of (Ibrahim, 1993), while REFPROP NIST uses the methodology developed by (Tillner-Roth & Friend, 1998a).

Artificial neural networks (ANNs) are a branch of artificial intelligence, based on brain behavior, more explicitly on biological neurons (Díez et al., 2001). Currently they are widely used in different fields of knowledge, ANNs are also defined as well-specified mathematical systems designed to capture the highest class of intelligence found in the brain, i.e. to capture the functional capacity of the system (Takeyas, 2007).

Therefore, in this work, we intend to apply a methodology based on an ANN for obtaining the thermodynamic property enthalpy of the ammonia-water mixture, in order to evaluate energy balances in industrial processes (Vera-Romero & Heard-Wade, 2017a, 2018).
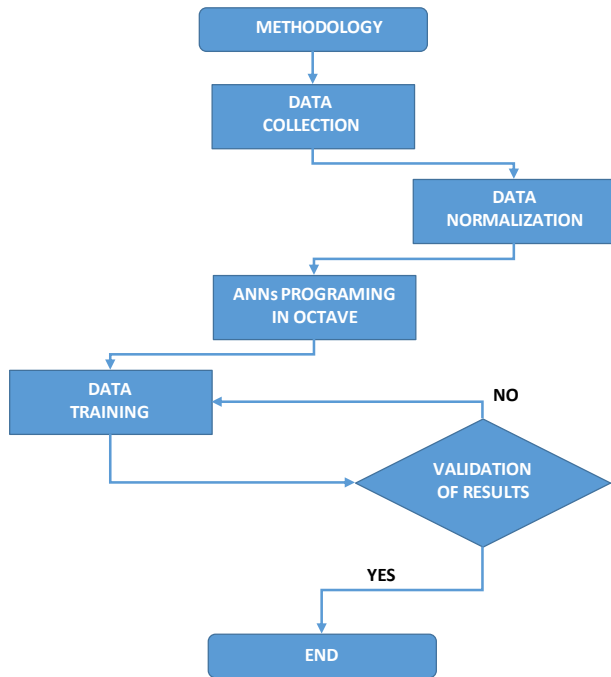
Methodology

For this work, we used the BackPropagation Network type (Maximiliano, 2019), which consists of learning a predefined set of input-output pairs given as an example (Bowen et al.; Dolling & Varas, 2002). First an input pattern is applied as a stimulus for the first layer of neurons in the network, it is propagated through all the upper layers until an output is generated, the result in the output neurons is compared with the desired output and an error value is calculated for each output neuron and to reduce this error it is validated through other methodologies. Two multilayer neural networks will be trained, Network A and Network B, which will have three input variables, Network A will have as input variables: Pressure (P), Temperature (T) and Ammonia Concentration (x), Network B will have as input variables: Pressure (P), mixture phase (q) and Ammonia Concentration (x), the networks will have two hidden layers for the connection of these variables and an output variable which is Enthalpy (h) as can be seen in Figure 1, showing the general network proposed for this work.
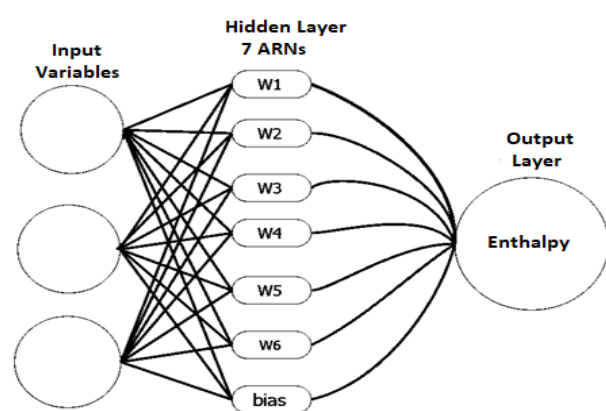
Figure 1 Proposed overall artificial neural network
Source: Own elaboration

The process for the realization of Network A and Network B can be basically divided into 5 main stages which are: data collection, data normalization, network programming, network training and validation of the results (fig 2).

Figure 2 Diagram of the methodology used
Source: Own elaboration

Stage 1, data collection

Experimental data reported in literature (Gillespie et al., 1985; Macriss, 1964; Park & Sonntag, 1990) were obtained to train the networks. The two ANNs have three input variables and one output variable, the networks share two input variables which are Pressure (P) and Ammonia concentration in the mixture (x), and have a different input variable, Network A has the variable Temperature (T) and Network B has the mixture phase variable (q).

The networks have the following characteristics

Each ANN has three sets of data for training and each set has two characteristics: each set has an isobar Pressure (P) and an ammonia Concentration (x) from 0 to 0.9999 where the only thing that varies is the Temperature (T) for Network A and the phase of the mixture (q) for Network B; and in each set of data the Concentration cycles again, this because the first part of the Concentration corresponds to the liquid state of the mixture and the second part corresponds to the gaseous state of the mixture.

For the two ANNs the Pressure (P) is isobar and in each network there are three different Pressures, i.e. a Pressure is set to find the results corresponding to each of the other two variables.

Subsequently, when the Pressure is fixed, the Concentration (x) is fixed and it is the third variable, either the Temperature (T) or the phase of the mixture (q), which ends up varying as well as the corresponding response variable (enthalpy). For the ammonia concentration (x) is taken from 0 to 0.9999 with intervals of 0.1. For the third set of data there is less data so the range of the concentration varies by 0.2.

For Network A, the Temperature corresponds to the Pressure and Ammonia Concentration of the experimental data used. The training pressures used were; 100 kPa, 200 kPa, 300 kPa, 5,000 kPa, 10,000 kPa and 11,000 kPa. For Network B, the third input variable used was the phase of the mixture (q), where it is defined as 1 if it is in liquid phase and 1 if it is in vapor phase, and the variable responds to the Pressure (P) and Concentration of the mixture (x). The training pressures used were; 5,000 kPa, 10,000 kPa and 11,000 kPa.

Stage 2, Data normalization

It is convenient to normalize the data before training a neural network. The normalization procedure consists of transforming the data so that they have a mean of 0 and a variance of 1 (eq. 1). Once the training is finished, denormalization should be used to return to the original domain of the data.

$$y = \frac{(X - X_{min})(d_2 - d_1)}{X_{max} - X_{min}} + d_1 \qquad (1)$$

Where:

X is the value to be normalized

$(X_{max} - X_{min})$ is the range of the value X

$(d_2 - d_1)$ is the range to which the value of X

y is the normalized value

Stage 3, programming of the RNA

The programming of the ANN was carried out through GNU Octave™, which is a free software and programming language for mathematical development, which can replace Matlab™ for free; and therefore the programming of the neural networks could be carried out in it.

At this stage, two programmings were made, one for the training and calculation of the weights and the other for the prediction of the enthalpy variable (h) for both networks.

Stage 4, ANN training

The training was handled in two parts: Weights and Error. The weights make the network learn which variable affects the result the most and what percentage of that variable will be used to arrive at the result.

A result variable is fed to compare with the result of the network, when comparing these results, an error is calculated and if the error is high, the weights are recalculated and rearranged, this process is repeated until a minimum error of 0.009 is obtained.

When the result of the network is the same or almost identical to that of the test variable, the network is considered to be trained (eq. 2-4).

$$E\% = \frac{EA}{DE} * 100 \qquad (2)$$

$$EA = VR - VP \qquad (3)$$

$$\sum EPP = \frac{\sum EA}{No.\ VR} * 100 \qquad (4)$$

Where:

$E\%$ = Percentage error

EA = Absolute error

DE = Exact data

$No.VR$ = Number of actual values

VR = Actual value

VP = Predicted value

$\sum EPP$ = Average percentage error

Stage 5, ANN Validation

Once the ANNs are trained, the enthalpy variable (h) is predicted for each network where the results must be validated for accuracy. Validation of the results is carried out against the EES software.

If there is no large discrepancy between results the ANNs will be taken as successfully trained and otherwise the networks must be retrained.

Results and discussion

Two artificial neural networks were created, Network A and Network B, both were multilayer Back Propagation type networks, each network has three independent input variables and a dependent output variable, which is the thermodynamic property of interest known as enthalpy (h). The results obtained from the training and their comparisons with the results obtained by the methodology of (Ibrahim, 1993) programmed in the EES are shown for each of the trained networks, as well as the prediction error for both networks.

NETWORK A

The first network corresponds to a Back Propagation network of multilayer architecture as shown in Figure 3, the network is composed of three independent input variables: Pressure (P), Temperature (T) and Ammonia concentration (x) and a dependent output variable which is the enthalpy (h).
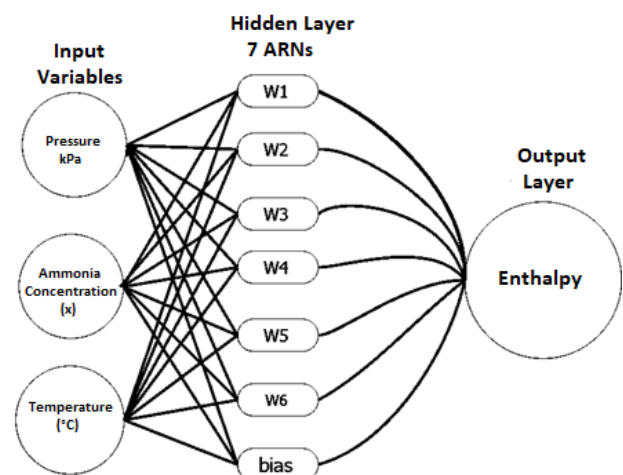
Figura 3 Red A Back multilayer propagation
Source: Own elaboration

For the training of this first network, the data were divided into three different groups, each with the corresponding values according to the output variable enthalpy (h), for each group corresponds a saturation pressure to which for each pressure corresponds a value of temperature (T) and a fraction of ammonia (x). The pressures used were 5,000 kPa, 10,000 kPa and 11,000 kPa.

The input variable data including the output variable enthalpy (h) were obtained from experimental data (Park and Sonntag, 1991).

The network was trained until an acceptable error was found between the result of the output variable and the data entered for training. The percentage error for this case is acceptable, which means that network A was adequately trained. To reach this acceptable error, the network was trained four times changing the epochs and the number of values to be compared with those of the training, the minimum error was obtained by training the network A 200 epochs and 60% of checking results. The epochs are the times that the neural network repeats the training process of the network. After this, the prediction of the enthalpy property (h) was performed, where three sets of data were predicted, that is to say, in the same way as for the training, for each set of data there is a Pressure (P) to which corresponds a value of Ammonia Concentration (x) and Temperature (T). Four predictions were made corresponding to 3,000 kPa, 5,000 kPa, 10,000 kPa and 15,000 kPa, for each group of predictions a Pressure in kPa is taken, the Temperature entered varies from 120 °C to 320 °C using intervals of 20 °C, for the Ammonia Concentration (x) data was used from 0 to 0.9999 with intervals of 0.1.

The validation of these results was carried out with the EES software, entering the same values of the input variables to the network, where the results yielded by the EES and those yielded by the neural network, in this first training, were incongruent. It was possible to verify that the temperatures used by the EES software are very far from those entered in the ANN, another aspect that was detected and that influenced the neural network to yield erroneous results was that the input data base for the training was too poor to obtain acceptable results.

As mentioned in the fifth step of the methodology, in case the prediction results had a large discrepancy with the results of the EES software, the ANN would be retrained until having a congruence of results with those of the EES. Therefore, enthalpy was calculated in EES at low pressures; 100 kPa, 200 kPa and 300 kPa added to the above to increase the range of data for training and prediction.

In order to lower the discrepancy in the results and increase the training values, the two neural networks created, Network A and Network B, were merged, since they shared 3 input variables; Pressure (P), Temperature (T) and Ammonia Concentration (x) and the variable that each network had a difference was added, resulting in 4 input variables; Pressure (P), Ammonia Concentration (x), Temperature (T), and phase of the mixture (q) in order to increase the database and have better training and prediction results, resulting in the multilayer network architecture as shown in Figure 4.
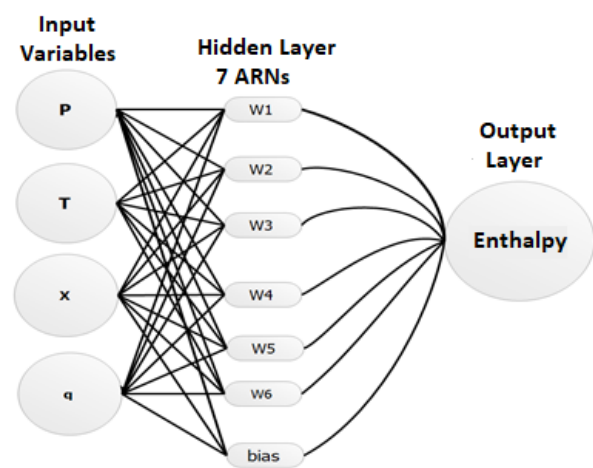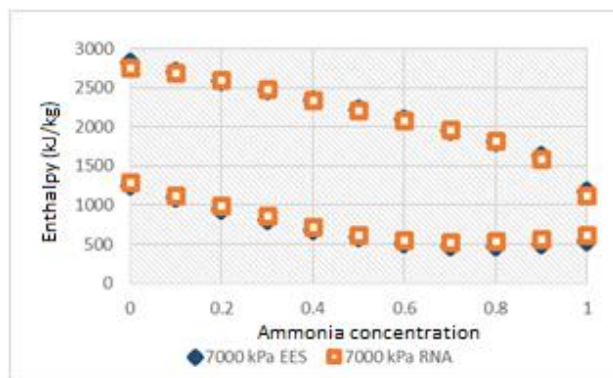

Figure 4 Modified multilayer network (Network A)
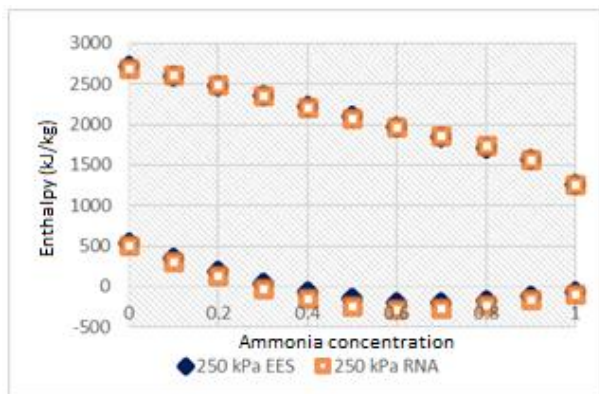*Source: Own elaboration*

Network A was retrained with the new input variable called mixture phase (q) and by adding pressures of 100 kPa, 200 kPa, and 300 kPa to the training database. Network A prediction was again made using pressures of 150 kPa, 250 kPa, 350 kPa, 3,000 kPa, 7,000 kPa, and 8,000 kPa, for which corresponds a value of Saturation Temperature (T), an ammonia concentration (x) from 0 to 1 with intervals of 0. 1, and a value of the enthalpy phase variable of -1 (saturated liquid) and 1 (saturated vapor), to validate again this Network A, the enthalpy results were compared with those of the EES software. Figures 5 to 10 show the comparison of the results for each pressure in a Concentration (x) vs Enthalpy (h) graph.
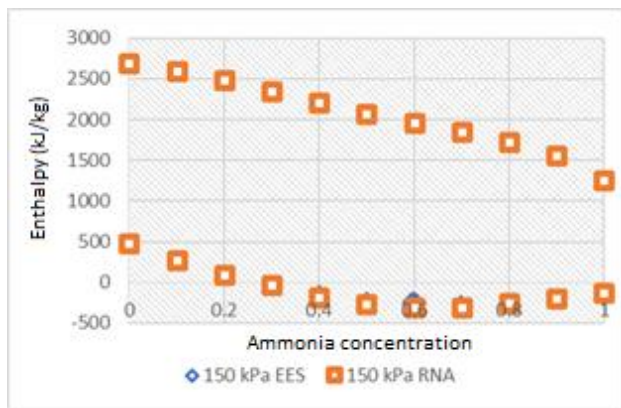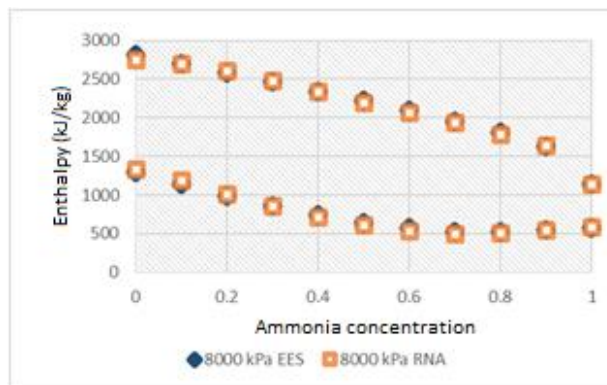
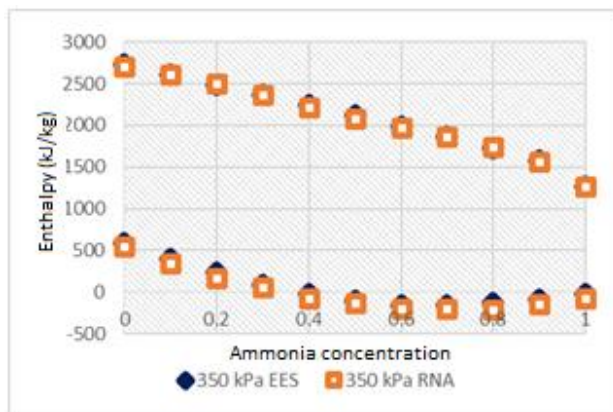**Figure 5** Network A vs EES at 150 kPa
Source: Own elaboration

Figure 6 Network A vs EES at 250 kPa
Source: Own elaboration

Figure 7 Network A vs EES at 350 kPa
Source: Own elaboration

Figure 8 Network A vs EES at 3,000 kPa
Source: Own elaboration

Figure 9 Network A vs EES at 7,000 kPa
Source: Own elaboration

Figure 10 Network A vs EES at 8,000 kPa
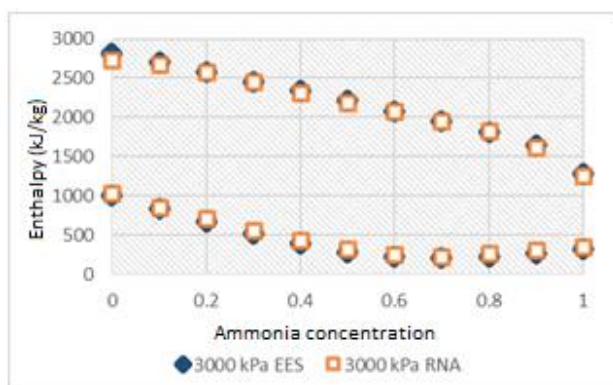*Source: Own elaboration*

The percentage error was plotted (Figure 11), where it is observed that the highest percentage of values are between the 0 error and the average percentage error resulting in 2.28%, which validates the ANN as trained and ready to make predictions that are between the range of 100 kPa and 10,000 kPa, the range may be higher or lower but within these values is where the highest prediction certainty is found.

Figure 11 Percentage error of results Network A vs. EES
Source: Own elaboration

VERA-ROMERO, Iván, PEREZ-AVIÑA, L. Fernando, MÉNDEZ-ÁBREGO, V. Manuel and MARTÍNEZ-REYES, José. Development of an artificial neural network for the prediction of the thermodynamic property enthalpy in the NH3-H2O mixture. ECORFAN Journal-Democratic Republic of Congo. 2022

After completing stage 5 of this work, which consisted of validating the ANN prediction with another methodology, in this case that of (Ibrahim, 1993), which is incorporated in the EES software, the general and specific objectives of this work were met, which consisted of creating an artificial neural network capable of predicting the thermodynamic property enthalpy in the binary mixture Ammonia-Water.

Discussion Red A

La Red A se entrenó a 100 kPa, 200 kPa, 300 kPa, 5,000 kPa, 10,000 kPa and 11,000 kPa and for each pressure corresponded a value of Temperature and Ammonia Concentration in the mixture, enthalpy property predictions were made at pressures of 150 kPa, 250 kPa, 350 kPa, 3,000 kPa, 7,000 kPa, and 8,000 kPa with their corresponding values of Temperature and Ammonia Concentration in the mixture. A total of 132 values corresponding to each input variable were predicted, these data were validated with the EES software with an average percentage error of 2.28%, where the highest percentage error value was 28.77 %. This is because the calculated enthalpy was at low pressures, e.g., at a pressure of 150 kPa, a temperature of 312.8 °C and an Ammonia concentration of 0.3, Network A predicted enthalpy of -23.91 kJ/kg while for EES it resulted in -19.06 kJ/kg, with an absolute error of the results of 4.85 kJ/kg and can be considered an acceptable variation for energy balances. However, the percentage error is 25.48 %, which is high, but justified by its equation which depends on the absolute error and the actual value, the lowest value of percentage error was 0.01425 %. The Red A is able to predict the enthalpy with results with a low range of acceptable error between 100 kPa and 10,000 kPa.

RED B

The second network corresponds to a Back Propagation network of multilayer architecture as shown in Figure 12, the network is made up of three independent variables and one dependent variable, the independent input variables are: pressure, enthalpy phase and ammonia concentration and the dependent output variable is the enthalpy.

Unlike Network A, in this network the independent variable Temperature is changed by the independent variable enthalpy phase (q); this variable is given two values which will depend on the phase in which the mixture is found, i.e. -1 for liquid phase and 1 for vapor phase.
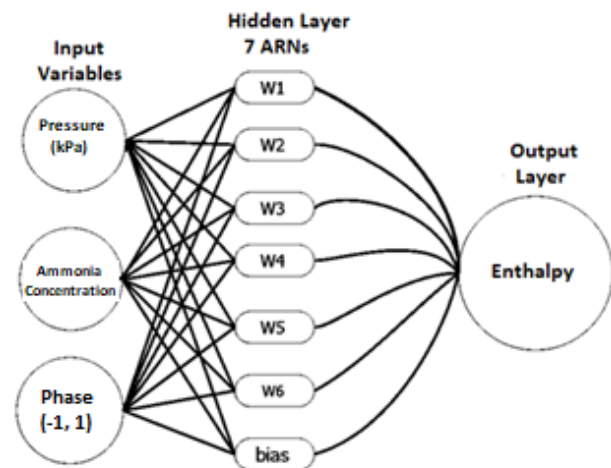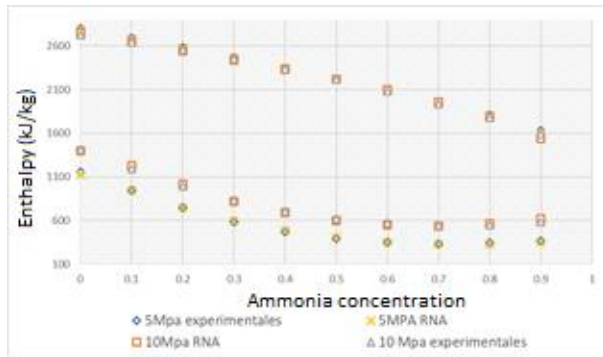

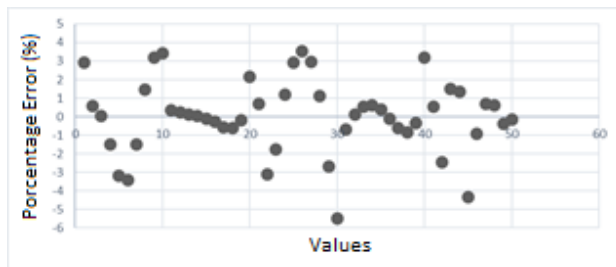**Figure 12** Network architecture B
Source: Own elaboration

In the same way that Network A was trained, in Network B the data were divided into three different groups, each set of data has the corresponding values according to the output variable enthalpy (h). For the first group of data the lowest pressure established in the literature of the experimental data of (Park & Sonntag, 1990) was taken, each group of data corresponds to a training pressure which are 5,000 kPa, 10,000 kPa and 11,000 kPa to each of them corresponded a value of ammonia concentration from 0 to 0.9 with intervals of 0.1 and a phase value of the mixture which is -1 if it is saturated liquid and 1 if it is saturated vapor.

Once the training of the network was finished, the resulting data were denormalized in order to have a better appreciation of them. With the denormalized data and once passed to a matrix in Excel™, the data entered for training were plotted against the training results of the network as shown in Figure 13; in which you can see the coincidence of the points and that they have the same behavior, which makes it clear that it was an acceptable training. Having the denormalized data, the percentage error was calculated as shown in Figure 14.

VERA-ROMERO, Iván, PEREZ-AVIÑA, L. Fernando, MÉNDEZ-ÁBREGO, V. Manuel and MARTÍNEZ-REYES, José. Development of an artificial neural network for the prediction of the thermodynamic property enthalpy in the NH3-H2O mixture. ECORFAN Journal-Democratic Republic of Congo. 2022

Figure 13 Experimental data (Park & Sonntag, 1990) vs Red B
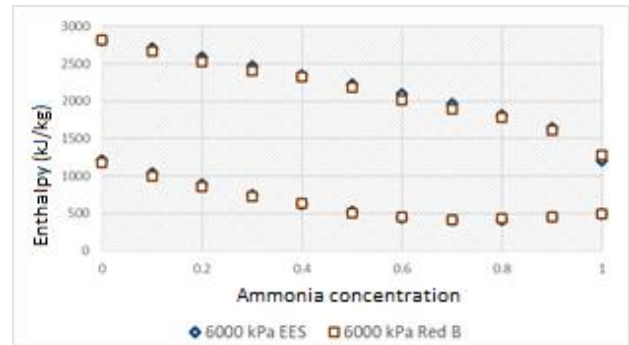*Source: Own elaboration*

**Figure 14** Percentage error of training Red B
Source: Own elaboration

Once verified that the training error is as close to zero as possible, the enthalpy prediction was made at two different pressures. The first prediction was made at a pressure of 6,000 kPa, the range of the ammonia concentration variable was from 0 to 0.9999 and for the mixture phase variable (q) it was in liquid and vapor phase (-1, 1).

The second prediction was made at a pressure of 7,000 kPa, the range for the variable ammonia concentration was from 0 to 0.9999 and for the variable mixture phase was liquid and vapor phase (-1, 1). The results of the prediction were plotted to see its behavior in a diagram Ammonia Concentration vs Enthalpy compared against the values obtained by the EES (Figures 15 and 16), which corresponds to a Pressure of 6,000 kPa and 7,000 kPa, where it can be observed that they have the same behavior shown in the Network A literature, so it can be concluded that the network performed a satisfactory prediction.

Figure 15 Results vs EES at 6,000 kPa, Network B
Source: Own elaboration
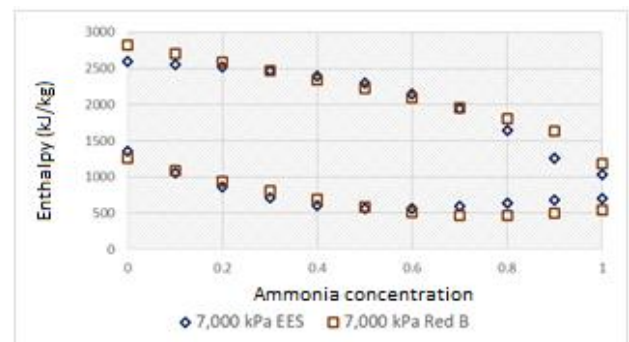
Figure 16 Results vs. EES at 7,000 kPa, Network B
Source: Own elaboration

Figure 17 shows the percentage error where it can be seen that most of the values are close to zero and the two most decentralized values were given when the ammonia concentration was one, this is because the EES takes the enthalpy of ammonia directly and the ANN takes the value calculated from the Network B training.
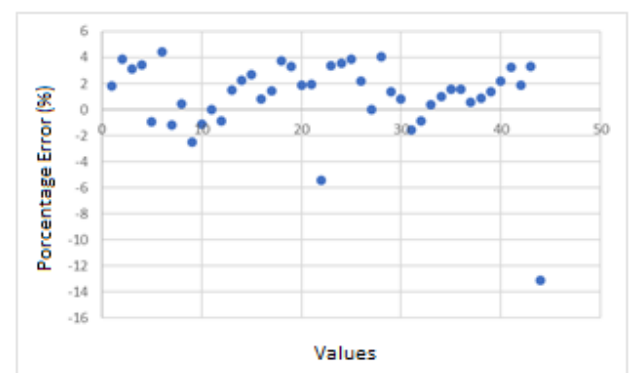
Figure 17 Percentage error in the validation between results vs. EES, Network B
Source: Own elaboration

Discussion Red B

As with Network A, the results were validated with the EES software (Ibrahim, 1993); detecting that the objective is met, which is to create an artificial neural network capable of predicting the thermodynamic property enthalpy in the binary mixture Ammonia-Water, for the realization of energy balances in various thermodynamic processes.

Network B was trained at 5,000 kPa, 10,000 kPa and 11,000 kPa and for each pressure corresponded a phase value of enthalpy (q) and Ammonia concentration in the mixture (x), enthalpy property predictions were made at pressures of 6,000 kPa and 7,000 kPa, with a total of 44 prediction values and an average percentage error of 2. 30 %, where the highest error value was 13.13 %, this is due to the fact that the values given when the concentration of Ammonia is 1 the Network B continues calculating according to its training, while the EES gives the direct value of the Ammonia property and not of the mixture. While the lowest percentage error value was 0.0204 %. Red B is able to predict the enthalpy with results with a low range of acceptable error between 5,000 kPa and 10,000 kPa.

Conclusions

Both Network A and Network B are capable of predicting the enthalpy property of the binary mixture Ammonia-Water, for the predictions of each network there was a low margin of acceptable error when validating the results with the EES software, however, for these predictions to be under an acceptable range of percentage error (0.01425% and 0.0204 %) they have to be predicted within a training pressure range for each network. That is, for Network A between 100 kPa and 11,000 kPa and for Network B between 5,000 and 10,000 kPa should be used. Although the networks can predict with an indefinite range, they only predict effectively if the range of the input variables is within the training values, therefore, the prediction of the neural networks will depend on the range of training values; the more robust the neural network is, the more accurate values it can predict and the more variables it can predict.

The network can be trained with three variables and it could predict, not only the enthalpy, but also: entropy, phase of the mixture, ammonia concentration in the mixture, water concentration in the mixture, temperature and pressure. This shows that ANNs are an alternative that is still little explored, but with a great potential for applications, not only to predict thermodynamic properties of this mixture, but of any type of binary or multicomponent mixture, the only limitation is to have sufficient data in wide intervals, since the networks are limited to the extrapolation of their training values.

References

Bowen, A. M., Telemática, I., & Asensio, H. G. Inteligencia artificial. Redes neuronales y aplicaciones. https://gc.scalahed.com/recursos/files/r161r/w25164w/M1CDN109_S5_Inteligencia_artificial_redes_neuronales.pdf

Díez, R. P., Gómez, A. G., & de Abajo Martínez, N. (2001). Introducción a la inteligencia artificial: sistemas expertos, redes neuronales artificiales y computación evolutiva. Universidad de Oviedo.

Dolling, O. R., & Varas, E. A. (2002). Artificial neural networks for streamflow prediction. Journal of Hydraulic Research, 40(5), 547-554. https://doi.org/10.1080/00221680209499899

Gillespie, P. C., Wilding, W. V., & Wilson, G. M. (1985). Vapor-liquid Equilibrium Measurements on the Ammonia-water System from 313 K to 589 K: A Join Research Report by the Gas Processors Association and the Design Institute for Physical Property Data of the American Institute of Chemical Engineers. Gas Processors Assoc.

Ibrahim, O. y Klein S. (1993). Thermodynamic properties of ammonia-water mixtures. ASHRAE Transactions: Symposia (Vol. 93, p. 1495). https://www.researchgate.net/profile/Osama-Ibrahim-15/publication/279905260_Thermodynamic_properties_of_ammonia-water_mixtures/links/607c7b09881fa114b410fcbf/Thermodynamic-properties-of-ammonia-water-mixtures.pdf

Kalina, A. I. (1983). Combined cycle and waste heat recovery power systems based on a novel thermodynamic energy cycle utilizing low-temperature heat for power generation. ASME Turbo Expo: Power for Land, Sea, and Air, 79368, V001T002A003. American Society of Mechanical Engineers. https://watermark.silverchair.com/

Macriss, R. A. (1964). Physical and thermodynamic properties of ammonia-water mixtures. Institute of Gas Technology. https://iifiir.org/en/fridoc/physical-and-thermodynamic-properties-of-ammonia-water-mixtures-1278

Maximiliano, E. (2019). Implementación de tecnologías basadas en Inteligencia Artificial para el análisis de la conducta de robots móviles autónomos en espacios de configuración en colisión Alejandro Armando H. DESARROLLO E INNOVACIÓN EN INGENIERÍA, 324.

Park, Y., & Sonntag, R. (1990). Thermodynamic properties of ammonia-water mixtures: a generalized equation-of-state approach. ASHRAE Trans, 96(1), 150-159. https://www.techstreet.com/standards/3319-thermodynamic-properties-of-ammonia-water-mixtures-a-generalized-equation-of-state-approach?product_id=1717225

Stecco, S. S., & Desideri, U. (1989). Thermodynamic analysis of the kalina cycles: comparisons, problems, perspectives. ASME 1989 International Gas Turbine and Aeroengine Congress and Exposition, 4, 1-8. American Society of Mechanical Engineers, ASME. https://watermark.silverchair.com/

Takeyas, B. L. (2007). Introducción a la inteligencia artificial. Instituto Tecnológico de Nuevo Laredo. Web del autor: http://www. itnuevolaredo. edu. mx/takeyas.

Thorin, E. (2000). Comparison of correlations for predicting thermodynamic properties of ammonia–water mixtures. International journal of thermophysics, 21(4), 853-870. https://link.springer.com/article/10.1023/A:1006658107014

Thorin, E. (2001). Thermophysical properties of ammonia–water mixtures for prediction of heat transfer areas in power cycles. International journal of thermophysics, 22(1), 201-214. https://link.springer.com/article/10.1023/A:1006745100278

Thorin, E., Dejfors, C., & Svedberg, G. (1998). Thermodynamic properties of ammonia–water mixtures for power cycles. International journal of thermophysics, 19(2), 501-510. https://link.springer.com/article/10.1023/A:1022525813769

Tillner-Roth, R., & Friend, D. G. (1998a). A Helmholtz free energy formulation of the thermodynamic properties of the mixture {water+ ammonia}. Journal of physical and chemical reference data, 27(1), 63-96. https://doi.org/10.1063/1.556015

Tillner-Roth, R., & Friend, D. G. (1998b). Survey and Assessment of available measurements on thermodynamic properties of the mixture {Water+ Ammonia}. Journal of physical and chemical reference data, 27(1), 45-61. https://doi.org/10.1063/1.556014

Vera-Romero, I., & Heard-Wade, C. L. (2017a). Comparación en las condiciones termodinámicas de operación de un sistema de refrigeración por absorción amoniaco-agua por primera y segunda Ley. SOMIM 2017, 118-128. http://somim.org.mx/memorias/memorias2017/

Vera-Romero, I., & Heard-Wade, C. L. (2017b). Desarrollo de una aplicación para el cálculo de las propiedades de la mezcla amoniaco-agua. Revista Ingeniería, Investigación y Desarrollo, 17(2), 58-72. http://repositorio.uptc.edu.co/handle/001/2441

Vera-Romero, I., & Heard-Wade, C. L. (2018). Evaluation of irreversibility in an ammonia-water absorption refrigeration system using three different mathematical models to calculate the thermodynamic properties. Revista Facultad de Ingeniería; Volumen 27, número 47 (Enero-Abril 2018). http://repositorio.uptc.edu.co/handle/001/2169

Rotor crack moment of inertia

Momento de inercia en fisura de rotor

JIMÉNEZ-RABIELA, Homero†*, VÁZQUEZ-GONZÁLEZ, Benjamín, RAMÍREZ-CRUZ, José Luis and ILIZALITURRI-BADILLO, Joshua Suraj

Universidad Autónoma Metropolitana, Unidad Azcapotzalco, División de Ciencias Básicas e Ingeniería, Departamento de Energía

ID 1st Author: *Homero, Jiménez-Rabiela* / **ORC ID** 0000-0002-1549-0853, **Researcher ID Thomson**: S-2299-2018, **CVU CONACYT ID**: 123386

ID 1st Co-author: *Benjamín, Vázquez-González* / **ORC ID**: 0000-0002-9030-5662, **Researcher ID Thomson**: S-2417-2018, **CVU CONACYT ID**: 25749

ID 2nd Co-author: *José Luis, Ramírez-Cruz* / **ORC ID**: 0000-0003-0762-2630, **Researcher ID Thomson**: G-3405-2019, **CVU CONACYT ID**: 921268

ID 3rd Co-author: *Joshua Suraj, Ilizaliturri-Badillo* / **ORC ID**: 0000-0003-2008-067X, **Researcher ID Thomson**: HGV-1387-2022

Abstract

The objective of this article is to evaluate the change in the moment of inertia of a rotor with chordal diagonal triangular crack, in all cross sections from the beginning to the end of it. The triangle used to generate the crack is isosceles and its inclination with respect to the transversal will be constant and equal to one sixth of π. The quotient of the width between the depth of the crack, from its birth and during its growth, is invariant and equal to 0.2. The ratio of the depth of the crack between the radius will vary from 0.4 to 0.6. The moment of inertia of the resulting cross-sectional area is calculated from the moments of inertia of component areas. Since in the antecedents there is information about cracks: transverse chordal rectangular, diagonal chordal rectangular, transverse chordal triangular; the present work expands the knowledge of the moment of inertia of the cracks to those that are triangular diagonal chordal; increasing the evidence for the subsequent early detection of cracks in rotors.

Rotor, Cracks, Moment of inertia

Resumen

El objetivo del presente artículo es evaluar el cambio en el momento de inercia de un rotor con fisura triangular diagonal cordal, en todas las secciones transversales desde el inicio hasta el fin de ésta. El triángulo usado para generar la fisura es isósceles y su inclinación con respecto a la transversal será constante e igual a un sexto de π. El cociente del ancho entre la profundidad de la fisura, desde su nacimiento y durante su crecimiento, es invariante e igual a 0.2. El cociente de la profundidad de la fisura entre el radio será variable de 0.4 a 0.6. El momento de inercia del área transversal resultante se calcula a partir de los momentos de inercia de áreas componentes. Puesto que en los antecedentes se encuentra información sobre fisuras: rectangulares transversales cordales, rectangulares diagonales cordales, triangulares transversales cordales; el presente trabajo expande el conocimiento del momento de inercia de las fisuras a aquellas que son triangulares diagonales cordales; incrementando los elementos de juicio para la ulterior detección temprana de fisuras en rotores.

Rotores, Fisuras, Momento de inercia

---

* Correspondence to Author (E-mail: hjr@azc.uam.mx)
† Researcher contributing first author.

Introduction

The evaluation of the moment of inertia of rotors in the cross sections corresponding to their cracking is important as it allows the early detection of cracking. The interest of the scientific community in the subject is noted by the publication of articles related to the topic, some of which are described below: A. Lazarus, et al (2008), applying eigenvalues and eigenvectors, as well as Floquet's theory and Mathieu's equation, studied rotating systems and their asymmetric rigidity. Ramezanpour, et al (2012), investigated the behavior of a Jeffcott rotor with diagonal crack in arbitrary orientation, using fracture mechanics concepts they determined the stiffness and flexibility matrices of the system. Ghozlane, M. (2015), proposed a simplified approach to model an open crack in a rotor based on the change of its flexibility. Gou, G. & Liu, C. (2016), determined the stiffness variation of a rotor containing a transverse crack. Fellah, A., Jadjoui, A. & Bakhaled, B. (2017), studied the effect of a transverse crack in a rotor taking into account the stiffness variation. Bakhaled, B., Jadjoui, A. & Fellah, A. (2018), proposed a new method, based on the theory of local stiffness decrease in a cracked rotor, to predict the presence of a crack. Jameel, A. & Thijeel, J. (2019), estimated the effect of a crack on the critical rotor speed using two methods: analytical and fast Fourier transform. Joseph, S. Helen, W. & Richard, Y. (2020), applied non-symmetric bending principles in rotor crack modeling without assuming horizontality of the neutral plane. Peter, K. & Robert, G. (2021), presented two simple methods to measure the moment of inertia of rotors without disassembly and without special laboratory equipment. Mohammad, A. & Fatima, K. (2021). They introduce an effective stiffness measure to analyze the effect of crack and unbalance force vector orientation on the negative potential intensity. Mo, Y. Hao, X, & Wei, X. (2022), Established an improved stiffness model of composite shaft crack based on layer theory, which considered the influence of orientation angle and stacking sequence of cracked layers.

The present work has added value in that, to date, no exact expressions have been published to determine the moment of inertia in the chordal diagonal triangular crack of a rotor.

The moment of inertia of the rotor cross sections, in its cracked zone, is obtained considering the rotor static and with the center of gravity of the crack on the axis with respect to which the moment of inertia is evaluated.

The exact evaluation of the moment of inertia in the cracked area will subsequently allow to know the global stiffness of the rotor and to predict more accurately its useful life. The following premise is assumed: Every geometry, however complex it may be, is composed of basic geometries.

Units and nomenclature are defined in the first section. Geometric calculations are described in the second section. The component areas are described in the third section. The moment of inertia of the component areas is determined in the fourth section. In the fifth section the moment of inertia for the area of interest is obtained. The results and conclusions are expressed in the sixth and seventh sections, respectively.

Units and nomenclature

Lengths in millimeters and angles in radians

Figure 1 shows the invariant input parameters. L = rotor length between supports, r = rotor radius. The origin of the inertial reference frame is at the center of the rotor at its initial cross section. The crack center is 0.5L from the origin of coordinates.
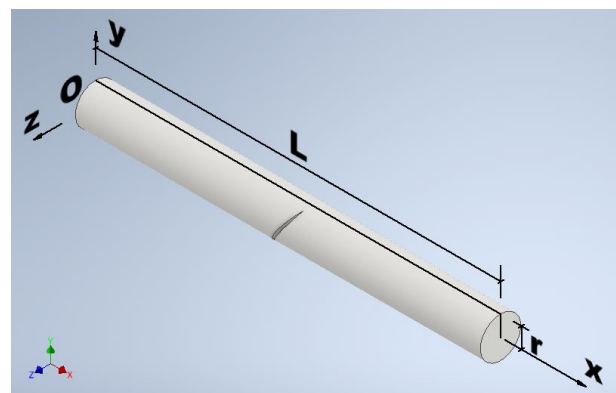
Figure 1 Cracked rotor
Source: Own elaboration

In Figure 2 the shear plane is obtained by rotating the xz-plane an angle around an axis 0.5L from the z-axis. Figure 3 shows the linear variable input parameters: a = crack width, p = crack depth. A, B, C and D are material points of the tool (isosceles triangle) used to generate the crack. E and F are material points on the crack edges, their distances to the rotor center are equal to r.
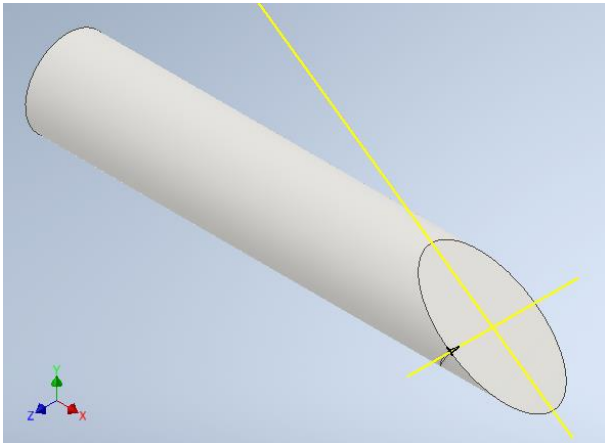

Figure 2 Diagonal cut
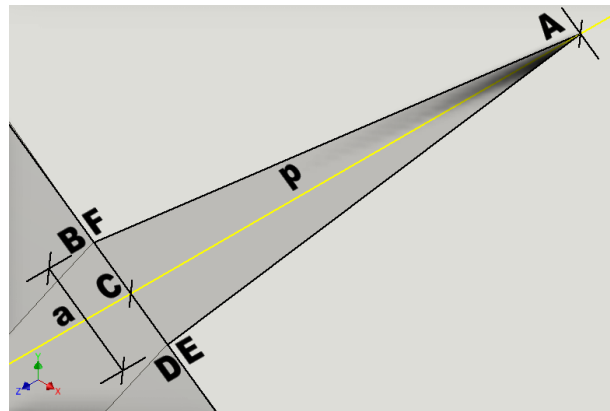*Source: Own elaboration*

Figure 3 Detail of Figure 2
Source: Own elaboration

Geometric calculations

In Figure 4 the shear plane is obtained by moving the xy plane a distance equal to r-p in the positive direction of the z-axis. Figure 5 shows the ith point A, where i will vary from 0 to 500, at the bottom of the crack, and from it the following equations are inferred:

$$y_{max} = \sqrt{2rp - p^2} \tag{1}$$

$$c = y_{max} Tg(\alpha) \tag{2}$$

$$x_{A_0} = 0.5L - c \tag{3}$$

$$x_{A_i} = x_{A_0} + i\frac{2c}{n} \tag{4}$$

$$x_{A_n} = 0.5L + c \tag{5}$$

$$d = \frac{x_{A_i} - x_{A_0}}{Tg(\alpha)} \tag{6}$$

$$y_{A_i} = d - y_{max} \tag{7}$$
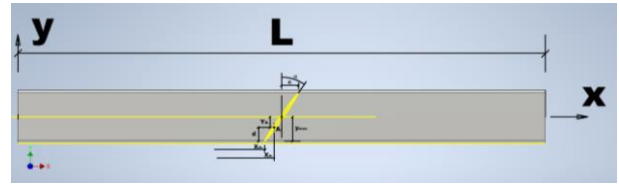
$$z_{A_i} = r - p \tag{8}$$

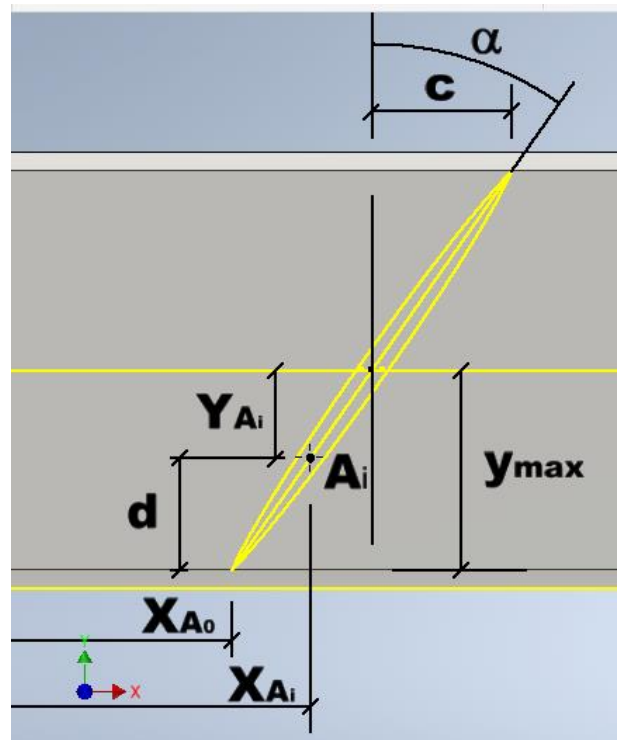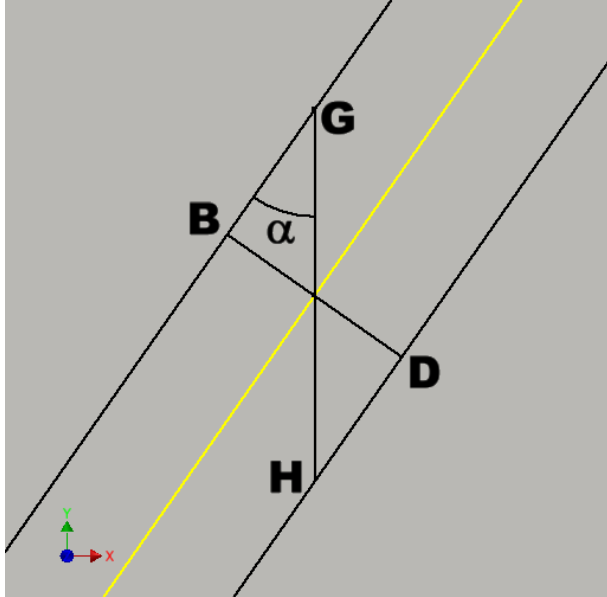**Figure 4** Crack front view
Source: Own elaboration

Figure 5 Detail of Figure 4
Source: Own elaboration

Figure 6 shows the tool in its path to generate the crack, from which the following equation can be inferred:

$$\overline{GH} = \frac{a}{sen(\alpha)} \tag{9}$$

Figure 6 Tool and crack
Source: Own elaboration

Figures 7 and 8 show both the panoramic and detail view of a cross section of the rotor. Point Q is the intersection of the x-axis with the extension of the line segment MA_i. Point S is the intersection of the x-axis with the extension of the line segment NA_i. If we denote with γ half of the angle GA_iH as shown in Figure 8, the following equations are obtained from the afore mentioned Figures:

$$\frac{y_{NA_i}}{z_{NA_i}} = Tg(\gamma) = \frac{0.5\overline{GH}}{p} \qquad (10)$$

$$y_{NA_i} = z_{NA_i}Tg(\gamma) \qquad (11)$$

$$(y_N)^2 + (z_N)^2 = r^2 \qquad (12)$$

$$\left[y_{A_i} + z_{NA_i}Tg(\gamma)\right]^2 + \left(z_{A_i} + z_{NA_i}\right)^2 = r^2 \qquad (13)$$

(13) becomes (14), (15), (16) and (17); with the solution given by (18).

$$A\left(z_{NA_i}\right)^2 + Bz_{NA_i} + C = 0 \qquad (14)$$

$$A = 1 + [Tg(\gamma)]^2 \qquad (15)$$

$$B = 2y_{A_i}Tg(\gamma) + 2z_{A_i} \qquad (16)$$

$$C = \left(y_{A_i}\right)^2 + \left(z_{A_i}\right)^2 - r^2 \qquad (17)$$

$$z_{NA_i} = \frac{-B + \sqrt{B^2 - 4AC}}{2A} \qquad (18)$$

Simultaneously the equation of the straight line through N and A_i with the equation of the z-axis yields.

$$z_S = \frac{Tg(\gamma)z_{A_i} - y_{A_i}}{Tg(\gamma)} \qquad (19)$$

A similar procedure is used to obtain:

$$y_{MA_i} = -z_{MA_i}Tg(\gamma) \qquad (20)$$

$$D = 1 + [Tg(\gamma)]^2 \qquad (21)$$

$$E = 2z_{A_i} - 2y_{A_i}Tg(\gamma) \qquad (22)$$

$$F = \left(y_{A_i}\right)^2 + \left(z_{A_i}\right)^2 - r^2 \qquad (23)$$

$$z_{MA_i} = \frac{-E + \sqrt{E^2 - 4DF}}{2D} \qquad (24)$$

$$z_Q = \frac{Tg(\gamma)z_{A_i} + y_{A_i}}{Tg(\gamma)} \qquad (25)$$

Using the above equations we obtain:

$$\theta_{A_i} = Arc\,Tg\left(\frac{y_{A_i}}{z_{A_i}}\right) \qquad (26)$$
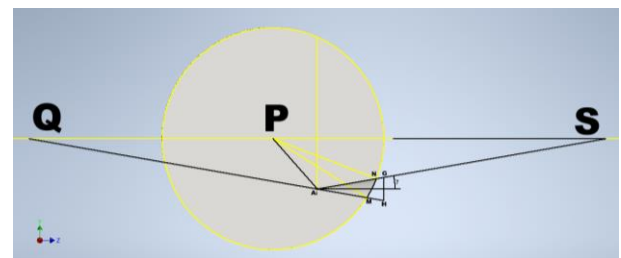
$$z_N = z_{A_i} + z_{NA_i} \qquad (27)$$

$$y_N = y_{A_i} + y_{NA_i} \qquad (28)$$

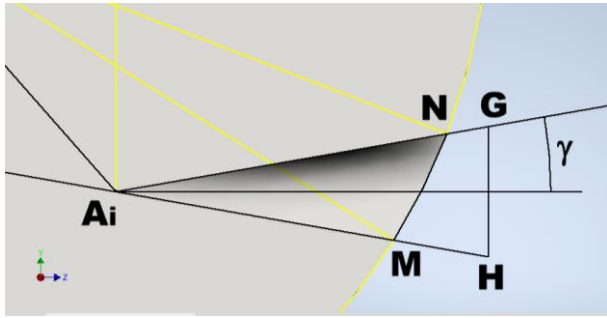$$\theta_N = Arc\,Tg\left(\frac{y_N}{z_N}\right) \qquad (29)$$

$$z_M = z_{A_i} + z_{MA_i} \qquad (30)$$

$$y_M = y_{A_i} + y_{MA_i} \qquad (31)$$
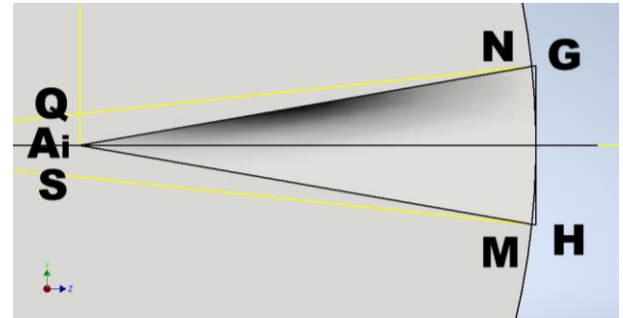
$$\theta_M = Arc\,Tg\left(\frac{y_M}{z_M}\right) \qquad (32)$$

Figure 7 Cross section i=100
Source: Own elaboration

Figure 8 Detail of Figure 7
Source: Own elaboration

Component areas

Based on the two previous Figures and the three subsequent Figures, it is possible to define basic component areas of the complex area whose moment of inertia is of interest.

The area defined by the arc MN and by the line segments PN y PM is subtracted from the area of the circle defined by the circumference of radius r. Subsequently the areas PA_iN and PA_iM are added or subtracted.

For i varying from zero to 250 there are two possibilities:

- The angle $\theta_{A_i} \leq \theta_M\_$M, the area PA_iN is to be added and the area PA_iM is to be subtracted.

- Angle $\theta_{A_i} > \theta_M$, area PA_iN must be added and area PA_iM must be added.

For i ranging from 251 to 500 there are two possibilities:

- The angle $\theta_{A_i} \leq \theta_N$, the area PA_iN must be summed and the area PA_iM must be summed.

- The angle $\theta_{A_i} > \theta_N$, the area PA_iN must be subtracted and the area PA_iM must be added.

The above component areas, in turn, are composite areas:

- $PA_iN = |PA_iS - PNS|$

- $PA_iM = |PMQ - PA_iQ|$

Figure 9 Cross section i=250
Source: Own elaboration
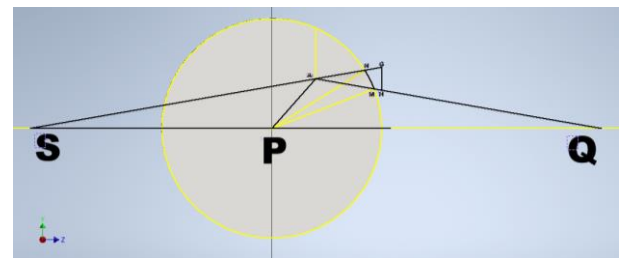
Figure 10 Cross section i=400
Source: Own elaboration
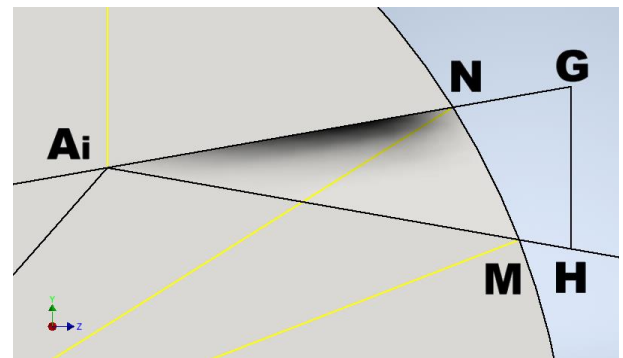
Figure 11 Detail of Figure 10
Source: Own elaboration

Moments of inertia of component areas

The moments of inertia of the component areas are as follows.

$$I_P = \frac{r^4}{8}[\theta_N - \theta_M + SC(\theta_M) - SC(\theta_N)] \quad (33)$$

$$SC(\theta_M) = sen(\theta_M)cos(\theta_M) \quad (34)$$

$$SC(\theta_N) = sen(\theta_N)cos(\theta_N) \quad (35)$$

$$I_{PA_iS} = \frac{|z_S||y_{A_i}|^3}{12} \quad (36)$$

$$I_{PNS} = \frac{|z_S||y_N|^3}{12} \quad (37)$$

$$I_{PMQ} = \frac{|z_Q||y_M|^3}{12} \quad (38)$$

$$I_{PA_iQ} = \frac{|z_Q||y_{A_i}|^3}{12} \qquad (39)$$
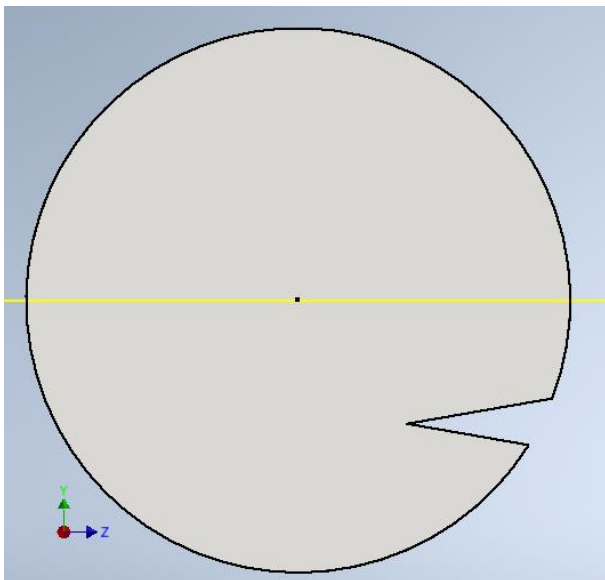
$$I_{PA_iN} = |I_{PA_iS} - I_{PNS}| \qquad (40)$$

$$I_{PA_iM} = |I_{PMQ} - I_{PA_iQ}| \qquad (41)$$

Where I_P is the moment of inertia of the circular sector bounded by the arc MN and by the line segments PM, PN.

Moment of Inertia of the Area of Interest

The area whose moment of inertia is to be determined is shown in Figure 12.

Figure 12 Area of interest
Source: Own elaboration

For i varying from zero to 250 and $\theta_{A_i} \leq \theta_M$:

$$I = I_c - I_P + I_{PA_iN} - I_{PA_iM} \qquad (42)$$

For i varying from zero to 250 and $\theta_{A_i} > \theta_M$:

$$I = I_c - I_P + I_{PA_iN} + I_{PA_iM} \qquad (43)$$

For i varying from 251 to 500 and $\theta_{A_i} \leq \theta_N$:

$$I = I_c - I_P + I_{PA_iN} + I_{PA_iM} \qquad (44)$$

For i varying from 251 to 500 and $\theta_{A_i} > \theta_N$:

$$I = I_c - I_P - I_{PA_iN} + I_{PA_iM} \qquad (45)$$

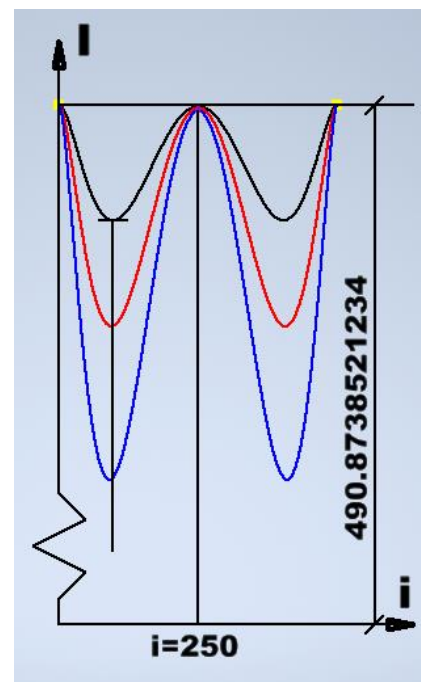Where the subscript c refers to the complete circle.

Results

For a rotor of a specific machine whose operating regime does not change in years; the linear input parameters L and r, can be considered invariant; for similar reason such a rotor will be subjected to both torsion and bending and the ratio of the tangential stresses among the normal ones, being invariant, will imply a constant angle α.

The depth and width will increase steadily from birth and throughout the crack growth.

The previous two paragraphs justified the treatment to each of the input parameters.

For all x_{A_i}, the following were determined:

- The coordinates (z, y) of A_i, N and M.

- The angles θ_{A_i}, θ_N y θ_M.

- Basic component areas (circle, circular sector and triangles).

- The moments of inertia of the areas of interest are shown in Figure 13 and complemented with Table 1.

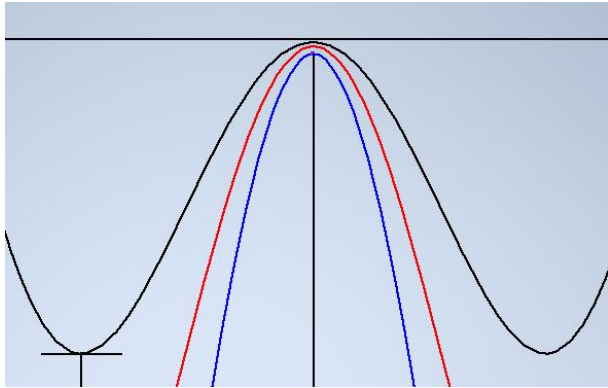**Figure 13** Moments of inertia
Source: Own elaboration

JIMÉNEZ-RABIELA, Homero, VÁZQUEZ-GONZÁLEZ, Benjamín, RAMÍREZ-CRUZ, José Luis and ILIZALITURRI-BADILLO, Joshua Suraj. Rotor crack moment of inertia. ECORFAN Journal-Democratic Republic of Congo. 2022

| Series	L	r	a	p	α
Black	100	5	0.4	2	1/6
Red	100	5	0.5	2.5	1/6
Blue	100	5	0.6	3	1/6

Table 1 Input parameters
Source: Own elaboration

Important relationships between the three series shown in Figure 13 can be seen in Figures 14 and 15.

Figure 14 Detail Figure 13 i=250
Source: Own elaboration

In the center of the crack the moment of inertia decreases as we increase the depth, maintaining zero slope in the center of the crack.
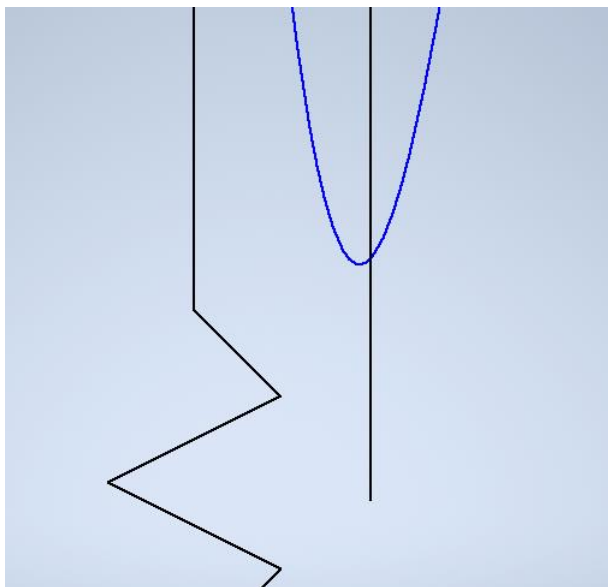
Figure 15 Detail Figure 13 lag
Source: Own elaboration

The vertical descending from the first minimum of the first series (black) passes slightly to the right of the first minimum of the third series (blue).

According to Figures 13, 14 and 15; Table 2 shows transcendent values of the presented series.

Series	I_{max}	I_{min}	I_{cf}
1	490.87	488.67	490.85
2	490.87	486.66	490.82
3	490.87	483.74	490.77

Table 2 Output parameters
Source: Own elaboration

Conclusions

The functional relationships presented allow to evaluate with accuracy and precision the moment of inertia of a rotor in all cross sections of its diagonal diagonal triangular chordal crack. Such relationships are applicable from the crack birth and during its growth; they constitute important elements of judgment in the early detection of cracks.

The results presented constitute an advance in the knowledge of the effect of a chordal diagonal triangular crack on the moment of inertia of a rotor. In this article the orientation of the crack was limited to the positive direction of the z-axis, in a later article it is convenient to evaluate the moment of inertia when the rotor is such and constantly modifies the orientation of the crack.

Acknowledgment

Funding

JIMÉNEZ-RABIELA, Homero, VÁZQUEZ-GONZÁLEZ, Benjamín, RAMÍREZ-CRUZ, José Luis and ILIZALITURRI-BADILLO, Joshua Suraj. Rotor crack moment of inertia. ECORFAN Journal-Democratic Republic of Congo. 2022

References

Lazarus, A. (2008). *Influence des dédauts sur le comportement vibratoire linéaire des systèmes tournants* (Tesis doctoral. Ecole doctorale de l'Ecole Polytechnique, Francia). Recuperado de http://www-cast3m.cea.fr/html/Theses_Cast3M/Lazarus.pdf

Ramezanpour, R., Ghayour, M. & Ziaei-Rad, S. (2012). Dynamic behavior of Jeffcott rotors with an arbitrary slant crack orientation on the shaft. *Applied and Conmputational Mechanics*, 6. Recuperado de https://pdfs.semanticscholar.org/21c3/0ebb2884 6d7dc29b2a5908c67a0e38d4d3ab.pdf?_ga=2.7 5022544.394348335.1584401537-1321827918.1583891375

Ghozlane, M. (2015). *Dynamic Response of Cracked Shaft in Rotor Bearing-Disk System*. Recuperado de: https://www.researchgate.net/publication/28189 0905_Dynamic_Response_of_Cracked_Shaft_i n_Rotor_Bearing-Disk_System

Guo, G. & Liu, C. (2016). Stiffness Variation of a Cracked Rotor with a Semi-Elliptical Front. En *School of Mechanical and Power Engineering, East China University of Science and Technology, Shanghai, China en International Conference on Sustainable Energy, Environment and Information Engineering*. Bangkok, Tailandia.

Fellah, A., Hadjoui, A. & Bakhaled, B. (2017). Numerical Study of an Open Cracked Rotor. En *IS2M Laboratory,Faculty of technology, University of Tlemcen, Algeria de la International Conference on Mechanical, Aeronautical and Industrial Egineering*. Paris, Francia.

Bakhaled, B., Hadjoui, A. & Fellah, A. (2018). AN ALTERNATIVE WAY TO PREDICT THE PRESENCE OF CRACKS IN A ROTOR BY STUDYING ITS VIBRATIONAL BEHAVIOUR. *U.P.B. Scientific Bulletin,* 80. Recuperado de: https://www.scientificbulletin.upb.ro/rev_docs_ arhiva/fullf72_29903.pdf

Jameel, A. & Thijeel, J. (2019). *Analytical Investigation of the Dynamics of Cracked Rotors* (Tesis doctoral. Baghdad University, Iraq). Recuperado de: https://www.researchgate.net/publication/33099 9316_Analytical_Investigation_of_the_Dynami cs_of_Cracked_Rotors

Joseph, S. Helen, W. & Richard, Y. (2020). *Application of Non-Symmetric Bending Principles on Modelling Fatigue Crack Behaviour and Vibration of a Cracked Rotor*. Recuperado de: https://www.researchgate.net/publication/33873 1385_Application_of_Non-Symmetric_Bending_Principles_on_Modelling _Fatigue_Crack_Behaviour_and_Vibration_of_ a_Cracked_Rotor

Peter, K. & Robert, G. (2021). *Measuring Mass Moment of Inertia of a Rotor-Two Simple Methods Using no Special Equipment*. Recuperado de: https://www.researchgate.net/publication/33799 0159_Measuring_Mass_Moment_of_Inertia_of _a_Rotor-Two_Simple_Methods_Using_no_Special_Equ ipment

Mohammad, A. & Fatima, K. (2021). *Negative potential energy content analysis in cracked rotors whirl response*. Recuperado de: https://www.ncbi.nlm.nih.gov/pmc/articles/PM C8316492/

Mo, Y. Hao, X, & Wei, X. (2022). *Analytical bending stiffness model of composite shaft with breathing fatigue crack*. Recuperado de: https://www.researchgate.net/publication/36163 8451_Analytical_bending_stiffness_model_of_ composite_shaft_with_breathing_fatigue_crack

Analysis of the use of aerogel as a thermal insulator in refrigerated containers for storing blood using a photovoltaic system

Análisis del uso de aerogel como aislante térmico en contenedores frigoríficos para almacenar sangre utilizando un sistema fotovoltaico

VALLE-HERNANDEZ, Julio†*, MANZANO-MUÑOZ, Meily Yoselin, ROMÁN-AGUILAR, Raúl and DELGADILLO-AVILA, Wendy Montserrath

Universidad Autónoma del Estado de Hidalgo. Escuela Superior de Apan, Ingeniería en Tecnología del Frío, México.

ID 1st Author: *Julio, Valle-Hernandez* / **ORC ID:** 0000-0001-89570066, **Researcher ID Thomson:** 0-7339-2018, **CVU CONACYT ID:** 210743

ID 1st Co-author: *Meily Yoselin, Manzano-Muñoz* / **ORC ID:** 0000-0002-2851-7998

ID 2nd Co-author: *Raúl, Román-Aguilar* / **ORC ID:** 0000-0003-0753-2352, **CVU CONACYT ID:** 165332

ID 3rd Co-author: *Wendy Montserrath, Delgadillo-Ávila*

Abstract

At the beginning of the present, a comparative analysis was carried out between polyurethane as a traditional thermal insulator and aerogel as an insulating material that has excellent thermal properties; the analysis is carried out through a container for storing blood, in which calculations of thermal loads were performed. In addition, a photovoltaic system is proposed to supply energy to the container. As a result, the energy consumption of the system is obtained, using the proposed insulators, resulting in lower consumption when aerogel is used.

Blood, Aerogel, Insulating

Resumen

Al inicio del presente, se realizó un análisis comparativo entre el poliuretano como aislante térmico tradicional y el aerogel como material aislante que posee excelentes propiedades térmicas; el análisis se realiza a través de un contenedor para almacenar sangre, en el cual se realizaron cálculos de cargas térmicas. Además, se propone un sistema fotovoltaico para suministrar energía al contenedor. Como resultado, se obtiene el consumo energético del sistema, utilizando los aislantes propuestos, resultando menor el consumo cuando se utiliza aerogel.

Sangre, Aerogel, Aislante

Citation: VALLE-HERNANDEZ, Julio, MANZANO-MUÑOZ, Meily Yoselin, ROMÁN-AGUILAR, Raúl and DELGADILLO-AVILA, Wendy Montserrath. Analysis of the use of aerogel as a thermal insulator in refrigerated containers for storing blood using a photovoltaic system. ECORFAN Journal-Democratic Republic of Congo. 2022. 8-15:19-24.

---

* Author Correspondence (E-mail: julio_valle@uaeh.edu.mx)
† Researcher contributing first author.

Introduction

Blood allows nutrition, communication, protection and repair of the various tissues of the organism, being of vital importance in operations and medical treatments. This leads to the need for blood banks, where its correct storage and transport must cover special characteristics, being the temperature one of the most important parameters that must be maintained from the moment it is donated until its conservation at 4°C.

An important problem in the storage processes is to choose the appropriate insulators to consume the least amount of energy to ensure the safety of the product to be preserved; that is why the objective of this work is to develop an analysis of the use of aerogel as thermal insulation in refrigerated containers to store blood and compare it with a traditionally used insulator, such as polyurethane; analyzing its implementation in a blood container in a theoretical way; such that allows to determine the greatest energy savings.

Methodology

The methodology to achieve the objective of this work consisted of seven steps.

In the first step, the geographic location of the blood storage enclosure is proposed; with this, the solar radiation and the maximum temperature at which the system will operate are determined. Step two consists of proposing the design of the container; geometry, measurements, materials, etc. Subsequently, in step three, the characteristics of the insulators for the case studies are specified. In step four, an energy analysis is performed to calculate the thermal loads, taking into account the amount of blood, the thermal insulation, the type of container material and air infiltration. In the fifth step the cooling source is chosen from the conditions obtained in the previous step. Step six consists of calculating the energy consumed by the chosen cooling system. Finally, in step seven, the photovoltaic system that provides the energy is selected.

Development

Climatic operating conditions

In order to establish the operating conditions, it is necessary to define a geographical location for the analysis. Although this work proposes the central region of the state of Hidalgo, where there is an average maximum ambient temperature of 21°C and a solar resource of 6.3 hours, the methodology presented can be extrapolated to any location.
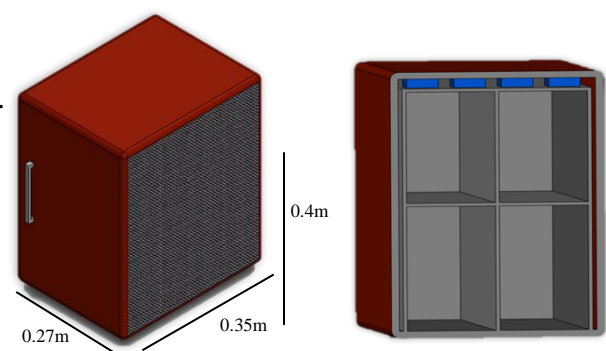
Container design

The size of the container was determined according to the amount of blood to be stored, which was 21 liters. Likewise, polypropylene was proposed as the material for its construction and for the insulating coating.

Table 1 shows the dimensions established for the container.

Dimension	Value
Height	0.4 m
Width	035 m
Long	0.27 m
Volume	0.04 m^3
Area	0.685 m^2
Material	**Thickness**
Polypropylene	0.254

Table 1 Container dimensions
Source: Own elaboration

Figure 1 shows the proposed design of the blood storage container.

Figure 1 Design and dimensions of the blood storage container
Source: Own elaboration

The container material was polypropylene for universal use, since it has excellent chemical resistance, high purity, low water absorption and good electrical insulation properties.

VALLE-HERNANDEZ, Julio, MANZANO-MUÑOZ, Meily Yoselin, ROMÁN-AGUILAR, Raúl and DELGADILLO-AVILA, Wendy Montserrath. Analysis of the use of aerogel as a thermal insulator in refrigerated containers for storing blood using a photovoltaic system. ECORFAN Journal-Democratic Republic of Congo. 2022

Insulation characteristics

One of the main disadvantages when refrigerating products is the heat transmission losses through the walls. One of the ways to reduce this heat loss is to select materials with low thermal conductivity, allowing the difference between internal and external temperatures to be maximized (Incropera, 1999).

Rigid expanded polyurethane foam is a lightweight, strongly cross-linked, closed-cell synthetic material with good mechanical strength relative to its density. This is one of the most widely used insulating materials because it reduces the energy consumption of the premises it protects, due to its good thermal insulation capacity (Acevedo, 2016).

On the other hand, aerogel is considered as the perfect thermal insulator. The main reason is that it is practically made of gases and, therefore, it is a material with low heat conductivity. It is able to cancel or drastically minimize the three existing heat transmission methods: conduction, convection and radiation (Gonzales, 2022).

Table 2 shows some characteristics of the insulators analyzed.

Insulation	Thermal conductivity W/mK	Specific heat KJ/Kg*K	Density Kg/m³
Polyurethane foam	0.028	1900	35
Silica aerogel	0.015	1.574	0.0004

Table 2 Insulation characteristics
Source: Own elaboration

Energy analysis

Thermal loads

The heat load is defined as the amount of heat that must be removed from the site to be cooled to reduce or maintain the desired temperature.

The total heat load results from the sum of the heat loads involved (HVACR, 2012). Based on the proposed design the thermal loads considered in this analysis are: by product, transmission through walls, and infiltration by outside air.

The temperature of the container must be maintained at 4ºC, considering a maximum temperature of 21ºC, corresponding to the case study.

Heat load per product

To calculate how much heat must be extracted from the device, the overall thermal load of the product is obtained as follows:

$$Q_{prod} = \left(\frac{m*Cp*\Delta T}{t}\right)$$

Where:

Q_{prod} = Heat extracted per product $[W]$.

m = Product mass $[kg]$.

Cp = Specific heat above freezing point $[KJ/kgK]$.

ΔT = Temperature difference $[K]$.

t = Time $[s]$.

Table 3 shows the parameters used to determine the thermal load per product.

Parameter	Value	Units
m	19.81	Kg
t	10800	S
Cp	3.8	kJ/kgK
ΔT	17	K

Table 3 Parameters to obtain the thermal load per blood product
Source: Own elaboration

Heat load generated by wall transfer

The thermal load generated by heat transfer through the walls of the container is calculated by the following equation:

$$Q_{walls} = A * U * \Delta T$$

Where:

Q_{walls} = Total heat transmission through walls $[W]$.

A = Heat transfer area $[m^2]$.

ΔT = Temperature differential between indoor and outdoor temperature [K].

U = Overall heat transfer coefficient [$[W/m]^2$ K], calculated as:

$$U = \frac{1}{\frac{1}{h_i} + \frac{e_1}{k_1} + \frac{e_2}{k_2} + \frac{1}{h_e}}$$

Where:

h = Convection coefficient [W/m²K].

e_n = Thickness [m].

k_n = Thermal conductivity [W/mK].

Table 4 shows the parameters used to determine the overall heat transfer coefficient.

Parameter	Value	Units
h_{inside}	10	W/m²K
$h_{outside}$	15	W/m²K
e_1	0.025	m
e_2	0.04	m
$k_{1polypropylene}$	0.2	W/mK
$k_{2polypropylene}$	0.028	W/mK
$k_{2aerogel}$	0.015	W/mK

Table 4 Parameters to determine U
Source: Own elaboration

Thermal load generated by air changes

The thermal load generated by air changes in the device is calculated by the following equation:

$$Q_{changes} = Q_2 = Q_{2.1} + Q_{2.2}$$

Where:

$Q_{2.1}$ = Heat load due to technical air renewal, [W] per day.

m_a = air mass [Kg/day].

V= Enclosure volume [m^3].

ρ= Average air density between indoor and outdoor conditions [Kg/m^3].

n = Number of technical renewals, renewals/day

Δh= Enthalpy difference between outside and inside air [W/kg]

$$Q_{2.2} = m_a * \Delta h$$

Being:

$$m_a = V * p * \theta$$

m_a= Infiltrated air mass, [Kg] per day.

V= Volume of infiltrated air [m^3].

ρ= Average air density between indoor and outdoor conditions [Kg/m^3].

θ= Door open time per day in seconds.

The volume of infiltrated air is a function of temperature and door dimensions:

$$V = \frac{a*H}{4} \sqrt{0.072 * H * \Delta T}$$

V = Air volume [m^3/s].

a = Door width [m].

H = Door height [m].

ΔT= Indoor/outdoor air temperature difference [K].

Total thermal load

The total thermal load is determined by the sum of the thermal loads considered, i.e. es:

$$Q_{total} = Q_{product} + Q_{walls} + Q_{changes}$$

Choice of cooling source

Once the total load that the system must remove to maintain operating temperatures has been calculated, a thermoelectric cooling system is chosen. This is because there is a small container and the volume can be cooled with a system of this type, which is environmentally friendly.

Table 5 shows the specifications of the Peltier cell chosen for the thermoelectric cooling system.

Specifications	
I max.	10 A
V max.	15.4 V
ΔT max.	150 °C
Q max.	89 W
Dimensions	40 x 40mm

Table 5 Specifications of a TEC-12710 Peltier cell
Source: Godoy, 2016

Energy consumed by the cooling system

With the universal performance graph it is possible to determine the current intensity at which the Peltier cell must operate in order to remove the heat from the system, and thus calculate the electrical power required to be supplied.
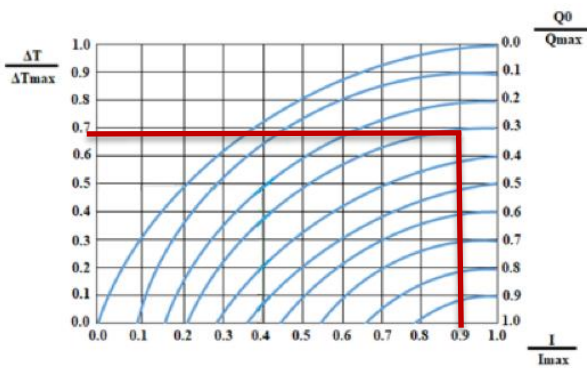
Figure 2 Universal yield curves
Source: Meerstetter Engineering, 2016

The Electrical Power required by the refrigeration system is calculated by the following equation:

$$P = V * I$$

Where:

P= Electrical power [W].

V= Maximum voltage [V].

I= Current intensity [A].

Choice of the photovoltaic panel

A light and flexible photovoltaic panel is proposed for quick installation and to provide the necessary energy for the operation of the system. Table 6 shows the specifications of the photovoltaic panel.

Parameter	Value	Units
Electrical power	250	W
Current	10	A
Voltage	12	V
Weight	0.862	Kg
Area	0.4	m^2

Table 6 Technical data sheet of the photovoltaic panel
Source: Own elaboration

To calculate the daily energy generated by the photovoltaic panel we have:

Energy = Panel power * Solar resource

Results

Table 7 shows the results of the thermal loads obtained for the container insulated with the two materials.

| Parameter	Value	Units
$Q_{product}$	119	W
Q_{wall_P}	8.40	W
Q_{wall_A}	4.89	W
$Q_{changes}$	13	W
Q_{total_P}	140.4	W
Q_{total_A}	136.89	W

Table 7 Total thermal load
Source: Own elaboration

Where:

Q_{wall_P} = Heat transmission through walls, using polyurethane as a thermal insulator.

Q_{wall_A} = Heat transmission through walls, using aerogel as thermal insulation.

Figure 3 shows the comparison between thermal loads by wall transmission for both insulating materials. It can be seen that in the case of aerogel the heat transmission is lower, being almost half that of polyurethane.

Thermal loads	Aerogel	Polyurethane	Unit
By walls	4.89	8.40	W
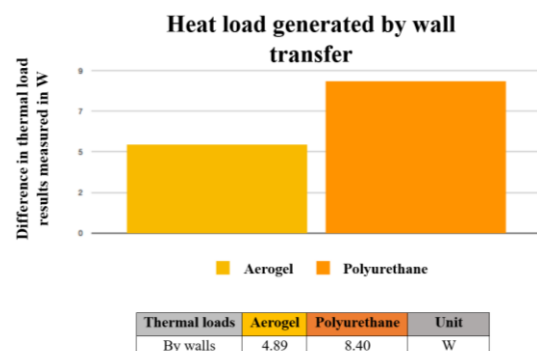
Figure 3 Graph of thermal load generated by wall transmission
Source: Own elaboration

With the total thermal load and considering five thermoelectrics, as specified in Table 5, the operating current of each one of them is obtained from the values shown in Table 8.

Parameter	Value	Units
ΔT_{max}	150	K
ΔT	17	K
Q_{max}	89	W
Q_{0A}	136.9/5	W
I_{max}	10	A
I	9	A

Table 8 Parameters to find the value of current intensity
Source: Own elaboration

With the value of the current intensity and the potential difference supplied by the photovoltaic panel we have a consumption of 108 W per thermoelectric. This gives a total of 540 W for the refrigeration system.

To cool the product from 21°C to 4°C, storage temperature, 1620 Wh are required. While to maintain the temperature of 4°C, 1134 Wh of energy is needed, giving a total of 2754 Wh per day.

The energy generated by two 250W photovoltaic panels, such as the one specified in Table 6, is 3150 Wh, which more than satisfies the 24-hour supply.

Conclusions

From the results obtained, it can be considered that the performance of the container is acceptable for the two cases of study; with polyurethane and aerogel as insulators. The difference between total thermal loads does not change significantly; however, aerogel, due to its low thermal conductivity, shows a notable difference in the thermal load through walls, since it is the only calculated load that has a direct relationship with the insulation.

In conclusion, we could observe that the use of aerogel as an insulator is not very important in small capacity containers, such as the one analyzed in this work, but it could be adequate for large containers, where the thermal loads through walls are significant. In this case study, the best option is to opt for polyurethane as insulation because of its lower cost.

References

BOHN (2005). Manual de ingeniería, recuperado de www.bohn.com.mx

Godoy Vaca, L. F. (2016). Diseño, construcción y evaluación energética de una cámara con celdas Peltier (efecto termoeléctrico) para refrigeración de vacunas. 130 hojas. Quito EPN

Çengel, Y. A., & Cimbala, J. M. (2012). Mecánica de fluidos: Fundamentos y aplicaciones (2a. ed.--.). México D.F.: McGraw Hill

Nasa Power. (2019). Prediction Of Worldwide Energy Resource. Recuperado de: https://power.larc.nasa.gov/data-access-viewer/

Solar fotovoltaica. (2002). Manuales sobre energía renovable: Solar Fotovoltaica. 1° Edición, 6-7

JRC Photovoltaic Geographical Information System (PVGIS) - European Commission. (2016, 11 enero). Recuperado 15 de octubre de 2022, de https://re.jrc.ec.europa.eu/pvg_tools/en/

Nuñez, I. U. (2021, 28 junio). ¿Qué son los aislantes térmicos? Características. Recuperado 15 de octubre de 2022, de https://www.xn--caractersticas-7lb.com/que-son-los-aislantes-termicos/

Acevedo, M. G. (2016). Caracterización de la espuma rígida de poliuretano expandido como impermeabilizante de cubiertas. https://www.redalyc.org/journal/1939/193946969001/html/

Gonzáles, A. (2022, 10 diciembre). Aerogel: el mejor aislante. Journal. Recuperado 15 de diciembre de 2022, de https://www.autodeskjournal.com/aerogel-el-mejor-aislante/

Design and 3D printing of the Robot, articulated with 6 degrees of freedom with educational applications

Diseño e impresión 3D del Robot, articulado de 6 grados de libertad con aplicaciones educativas

SÁNCHEZ-GUARNEROS, Raziel†*, MARTÍNEZ-HERNÁNDEZ, Haydee Patricia*, CORTES-MALDONADO, Raúl and BEDOLLA-HERNÁNDEZ, Jorge

Departamento de posgrado, Maestría en Ingeniería mecatrónica. Tecnológico Nacional de México/Instituto Tecnológico de Apizaco. Av. Instituto Tecnológico No. 418, San Andrés Ahuashuatepec, Municipio de Tzompantepec, Tlaxcala, México.

ID 1st Author: *Raziel, Sánchez-Guarneros* / **ORC ID:** 0000-0003-4550-4299, **CVU CONACYT ID:** 1153077

ID 1st Co-author: *Haydee Patricia, Martínez-Hernández* / **ORC ID:** 0000-0001-8863-4689, **CVU CONACYT ID**: 353253

ID 2nd Co-author: *Raúl, Cortés-Maldonado* / **ORC ID:** 0000-0001-8463-1325, **CVU CONACYT ID:** 335473

ID 3rd Co-author: *Jorge, Bedolla-Hernández* / **ORC ID:** 0000-0003-3856-6061, **CVU CONACYT ID:** 83901

Abstract

This work presents the complete manufacturing of an articulated robot of 6 degrees of freedom, with educational applications. With the purpose of increasing the motivation of the students in the significant learning of the subject of robotics. The methodology was developed from the design of each link of the robot in Solid Word, to later print it in 3D, followed by the mechanical and electrical/electronic implementation. In accordance with this, we worked with the mathematical modeling through the RoboAnalyzer software based on the Denavit Hartenberg parameters. To control the robot, so that the student has options to be able to control the robot, a control card was developed which is compatible with: Raspberry, Arduino and PIC microcontroller. In addition to the above possibilities of programming, another programming option is provided to only manipulate the robot with an application on a laptop, tablet or cell phone, these applications are free; it refers to Universal Gcode Sender and Bluetooth Electronics that simulate a teach pendant. With the development of this robotic equipment, it is intended to form integral students in their technological assets.

Resumen

Este trabajo presenta la manufactura completa de un robot articulado de 6 grados de libertad, con aplicaciones educativas. Con la finalidad de incrementar la motivación de los estudiantes en el aprendizaje significativo de la asignatura de robótica. La metodología se desarrolló desde el diseño de cada eslabón del robot en Solid Word, para posteriormente imprimirlo en 3D, a continuación, se realizó la implementación mecánica y eléctrica/electrónica. En concordancia con esto se trabajó con el modelado matemático a través del software RoboAnalyzer basándonos en los parámetros de Denavit Hartenberg. Para controlar el robot, de manera que el estudiante tenga opciones de poder controlar el robot, se desarrolló una tarjeta de control la cual es compatible con: Raspberry, Arduino y microcontrolador PIC. Además, de las anteriores posibilidades de programar, se brinda otra opción en programación de sólo manipular el robot con una aplicación en laptop, Tablet o teléfono celular, estas aplicaciones son libres; se refiere a Universal Gcode Sender y Bluetooth Electronics que simulan una teach pendant. Con el desarrollo de este equipo robótico se pretende formar estudiantes integrales en su haber tecnológico.

RoboAnalyzer, Raspberry, Arduino, PIC Microcontroller, Universal Gcode Sender, Bluetooth Electronics

RoboAnalyzer, Raspberry, Arduino, Microcontrolador PIC, Universal Gcode sender, Bluetooth Electronics

---

---

* Correspondence to Author (email: haydee.mh@apizaco.tecnm.mx)

† Researcher contributing first author.

Introduction

The education in some institutions that do not have equipped laboratories, practical subjects are offered, only with theory or simulations, this affects the student in their academic and work performance. The subject of robotics is very necessary in the Curriculum Vitae (CV) of engineers, as it is very required in the industry [1]. Because all industrial processes are being automated by robots, which have the tendency to replace man in heavy, monotonous or dangerous tasks.

Great scientists, engineers, athletes etc. have always said that practice makes the difference [2]. This leads us to understand that our educational institutions must teach the subjects in a practical way, with industrial equipment as close to reality as possible. For some institutions this equipment is complicated because they are very expensive or very difficult to install and a mistake could cause material or physical damage. We questioned how to innovate the way in which the subject of robotics is taught and learned, simulations are used and correct for the teaching of direct and inverse kinematics, however, the physical equipment is always required, so we implemented the articulated robot of 6 degrees of freedom to provide great support to the subject of robotics, and that students can program and manipulate a robot professionally and/or remotely as they would with an industrial robot, as well as provide options to program it through controller cards and increase student creativity so they can create projects that have an impact on their communities.

Objective

To design, implement and control an industrial scale robot for educational and training purposes.

Methodology

Robot design and printing

We developed a robot with our own design inspired by the BCN 3D ROBOT robot [3] with some improvements adapted to our needs, Figure 1.

For the 3D modeling of the robot we used free software such as BLENDER (Figure 2) and also Solidworks software since they are suitable for our design needs of each mechanical component.
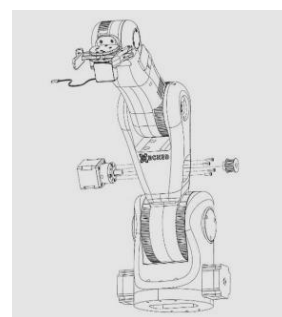

Figure 1 3D model of the robot (planetary gearing system)
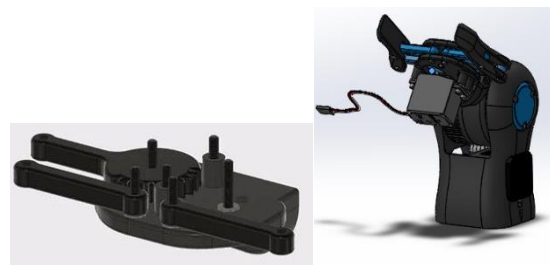
Figure 2 3D modeling of the gripper and the BCN 3D robot

Having the robot design to scale with the correct dimensions and tolerances of each part, its mechanical implementation was simulated to corroborate that the assembly will be correct, Figure 3.

Figure 3 Mechanical implementation of the BCN 3D robot

Once it is corroborated that all the pieces match perfectly, the printing of each one of the pieces in 3D printers begins, with an approximate printing time of 5 days (figure 4).
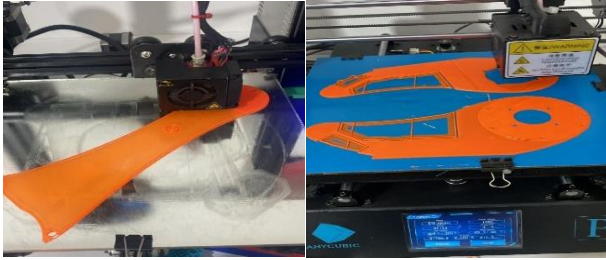
Figure 4 3D printing of the rotating column

Mechanical System

The 6 degrees of freedom articulated robot is composed of high performance motors with excellent flexibility and reliability. It is a unique slim design that reduces the space it occupies, allowing it to work in very narrow spaces. The robot is kept in balance on its base, thanks to a mechanical differential. The components of the ROBOT are as follows:

- Type: Articulated

- Number of axles: 6

- Degrees of freedom

- Maximum load: 20 Kg

- Minimum load: 5 Kg

Electrical/Electronic System

Each joint of the robot is controlled by stepper motors that allow them to have independent movements with a gearing system that increases the torque and creates a natural motion [4,5,6]. Table 1 shows the stepper motors that control the Robot's movements:

Stepper motor	Features	Source: (STEPPERONLINE 2022).
Nema 23	Bipolar 1.8 grados 2.4Nm (340oz.in) 1.8A 4.95V 57x57x104mm 4 Hilos.	
Nema 14	Bipolar L = 33 mm with gear ratio 51: 1 Planetary gearboxes.	
Nema 17	Bipolar L = 33 mm with gear ratio 27: 1 Planetary gearboxes.	

Table 1 Motor characteristics

The controllers or drivers used in the control of the motors are shown in Figures 5, 6 and 7:
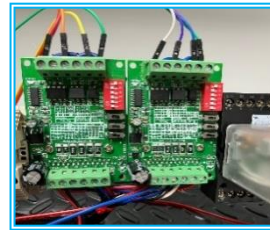

Driver TB6560
- o   Operating Voltage: 10 – 35 Vcd
- o   Current setting control
- o   Max Current: 3 A
- o   Pitch adjustment: 1, 1/2, 1/8 y 1/16
- –   •Compatible con shield match3 y Arduino (GRBL)

Figure 5 TB6560 Driver mounted in the control section

Driver A4988
- • Input Voltage 3.3v y 5v
- • Maximum Current 2A (Heatsink and ventilation).
- • Maximum Voltage: 35v
- • With heatsink
- • Step resolution: 1, 1/2, 1/4, 1/8 y 1/16.
- • Size 20 x 15 mm.

Figure 6 Driver A4988
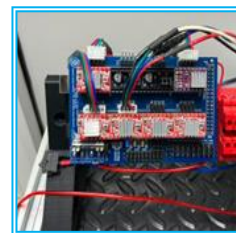
Driver 8825
-Logic voltage: 3.3V - 5V DC
-Power Voltage: 8.2V - 45V DC
-Current: 1.5A per coil (max. 2.2A)
-STEP and DIRECTION control interface
-6 resolutions: full step, half step, 1/4, 1/8, 1/16, 1/32, 1/16, 1/32
-Potentiometer allows you to limit the maximum current, so you can use higher voltages and achieve better resolution.
-Regulator included

Figure 7 Driver 8825 montado en la sección de control.

Control System

For the control of the robot, a control mother board was designed that is compatible with Arduino, PIC Microcontroller, Raspberry, in order to expand the options to control the actuators. Therefore, the following characteristics of this board are shown below:

- Controls up to 8 stepper motors simultaneously.

- Connection of up to 8 limit switches for homing motors.

- 1 PWM output signal for tool control.

- 12V auxiliary pin.

- 5V auxiliary pins.

This board is an Arduino shield and is connected to the Arduino through the digital pins. The complete electrical schematic is shown in Figure 8.
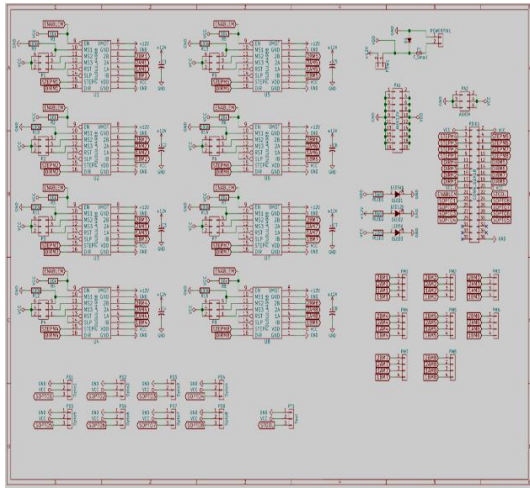
Figure 8 Control board electrical schematic diagram

In addition, for the control system, the cards were adapted to provide 2 robot manipulation options: the UGS program (Universal Gcode Sender) [7], the operator can manipulate the robot by means of commands programmed in G code (numerical control), shown in Figure 9.
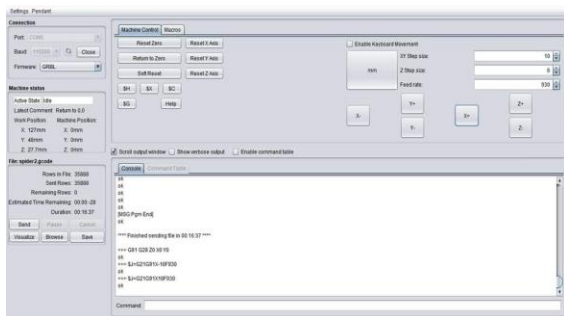

Figure 9 UGS software

It also provides the function of being able to manipulate the robot with a smartphone or tablet through the Bluetooth HC-05 module installed on the board, this is controlled through the free access application Bluetooth Electronics, see figure 10.
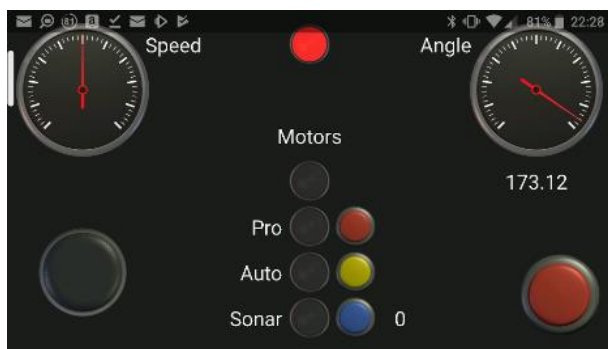
Figure 10 Aplicación Bluetooth electronics

Mechanical and Electrical/Electronic Implementation

Once we have each of the robot parts printed, we start with the mechanical assembly and electronic wiring, as shown in Figures 11 and 12.

Figure 11 3D printed parts (oscillator arm and neutral arm)

Figure 12 Stepper motor wiring

Results and tests

At the conclusion of the mechanical and electrical/electronic implementation stage, Figure 13 shows the Robot that is fully assembled and ready for programming.
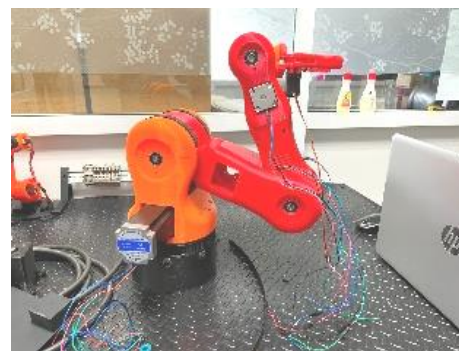

Figure 13 Implemented robot

The installation in the robotic trainer cell was carried out with the purpose of checking that each of the robot joints correspond to the dynamic movements according to the requested programming [8], this is shown in Figure 14.

Figure 14 Trainer robotic cell

Simulation of the mathematical modeling

For the mathematical modeling, RoboAnalyzer was used, which is a free software to simulate the mathematical modeling of the robot, shown in Figure 15.
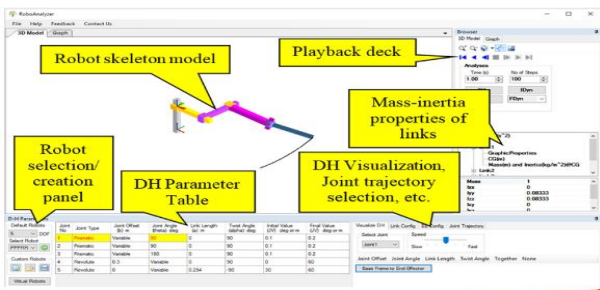

Figure 15 Main screen of the software, image from the cited article
Source: [9]

The mathematical modeling and simulation presented allow predicting the motion of each of the links without having to go to the physical system to obtain their final matrices [10], the calculation is based on the Denavit Hartenberg (DH) parameters. In addition, robot kinematics requires matrix algebra, coordinate transformations and multivariate equations [9]. Figure 16.
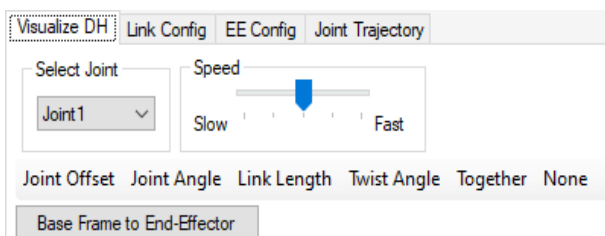

Figure 16 Parameters based on Denavit Hartenberg

When DH parameters are described mathematically, they are associated with coordinate transformations; the next thing is to understand their effect on the physical configuration of the robot, Figure 17, i.e., how a change in DH parameters can affect the robot architecture and vice versa. [9].
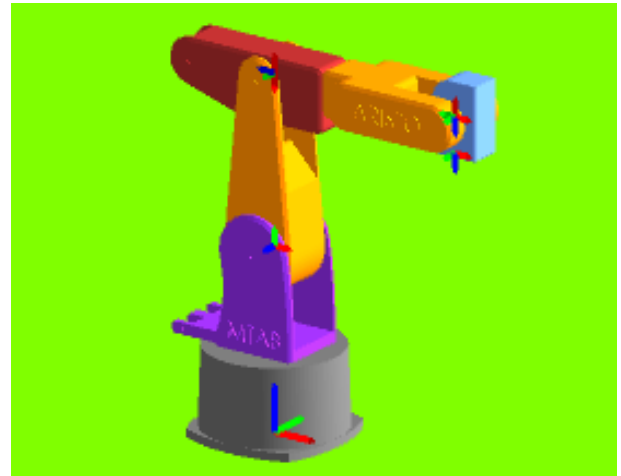

Figure 17 Visualization of DH parameters in RoboAnalyzer of the robot BCN-3D

To visualize the shapes of the robot's motion, the motion matrices to be moved by each joint and link are calculated. Otherwise, kinematically and dynamically, they are the same. Then the link parameters can be varied by changing the DH parameters to see the effects on the kinematic and dynamic performance.

This provides students with a way to explore variations on the given architecture of an industrial robot. [9].

i	$b_i(m)$	$\theta_i(°)$	$a_i(m)$	$\alpha_i(°)$		i	$b_i(m)$	$\theta_i(°)$	$a_i(m)$	$\alpha_i(°)$
1	0	0	0.1	0		1	0.1	0	0.1	90
2	0	0	0.125	0		2	0.1	0	0.125	90
3	0	0	0.1	0		3	0.1	0	0.1	90

Table 2 Variations in the BCN-3D robot articulations

As in this case the BCN 3D robot is a 6 degrees of freedom robot, we select the 6 degrees of freedom and the similar robot type. The chosen one is Aristo, and we verify that it is the required model (figure 18), therefore, we click on the green button, figure 19. The values are added in DH table (figure 15) of each of the links. Figure 19.
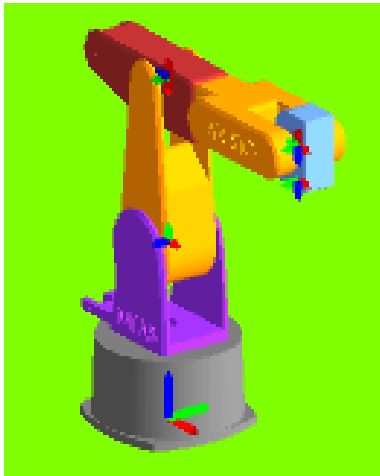
SÁNCHEZ-GUARNEROS, Raziel, MARTÍNEZ-HERNÁNDEZ, Haydee Patricia, CORTES-MALDONADO, Raúl and BEDOLLA-HERNÁNDEZ, Jorge. Design and 3D printing of the Robot, articulated with 6 degrees of freedom with educational applications. ECORFAN Journal-Democratic Republic of Congo. 2022

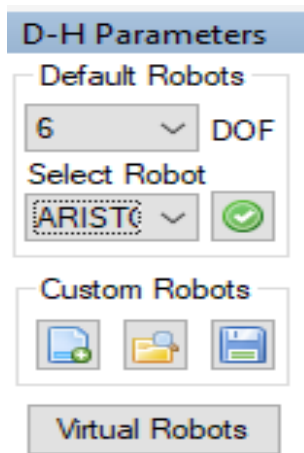**Figure 18** Aristo model, similar to the robot BCN 3D

Figure 19 Selection of robot characteristics

Joint No	Joint Type	Joint Offset (b) m	Joint Angle (theta) deg	Link Length (a) m	Twist Angle (alpha) deg	Initial Value (JV) deg or m	Final Value (JV) deg or m
1	Revolute	0.322	Variable	0	90	0	60
2	Revolute	0	Variable	0.3	0	90	60
3	Revolute	0	Variable	0	90	180	150
4	Revolute	-0.375	Variable	0	90	-180	-200
5	Revolute	0	Variable	0	90	-90	60
6	Revolute	0.063	Variable	0	0	0	60

Table 2 Table to insert DH values for each joint and linkage

Once the required parameters have been configured, select the FKin button to update the program memory. Then we select the play button to execute the required robot motion program. Figure 20.
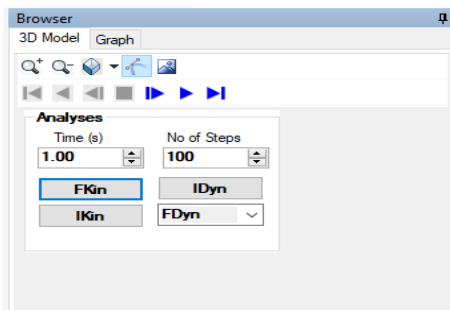

Figure 20 Buttons for executing robot movements

Then, the BCN 3D robot displayed on the screen will execute the calculated strokes of each joint according to the data entered in the DH table. Figure 21.

Figure 21 Movement of each joint of the robot

Subsequently, to analyze the resulting matrix, select the Link Config. option and choose the joint to be analyzed to display its DH matrix. Figura 22.
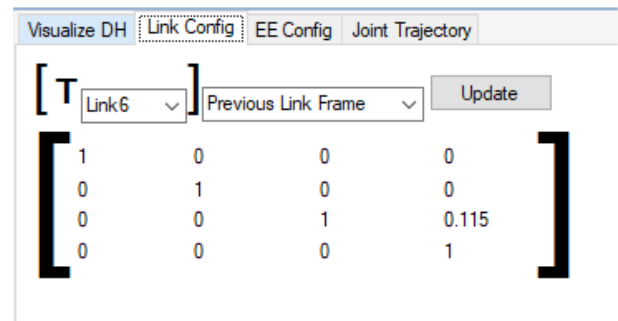

Figure 22 Display of the selected link matrix

The numerical values of the 4×4 homogeneous transformation matrices (HTMs) are necessary for kinematic and dynamic analyses, as they describe the position and orientation of the robot links. The RoboAnalyzer software and the HTMs for different links are available to the user in the GUI. This would allow them to validate their results, especially in the classroom and during practical exercises. [9,11]. Figure 23.
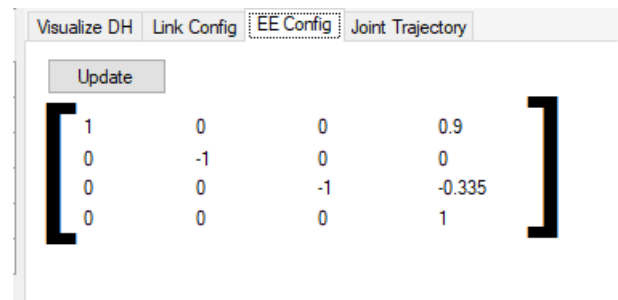

Figure 23 Homogeneous transformation matrix

The physical robot will match the movements, as the traces observed in the simulation, because the degrees that were entered in the DH table of the RoboAnalyzer software for each joint are the same degrees that were entered in the Universal Gcode Sender (UGS) software.

The trajectory of the cycloidal traces of the position of a joint and its corresponding velocity and acceleration are shown plotted in the Graph option. Figure 24.
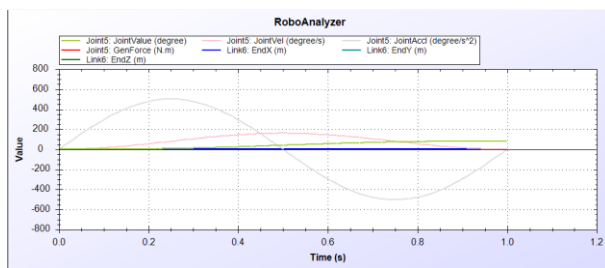
Figure 24 Plotted values of the final matrix of the BCN 3D robot

In this sense, when interpreting data and information, the mathematical modeling of a physical system refers to the process of obtaining a set of equations of this. From the point of view of the scope of what is required to simulate the system, this is how the trajectories of each link are obtained by means of mathematical equations. [9,11,12].

Conclusion

In this project the proposed objectives were satisfactorily achieved, with the purpose that the student interacts with equipment that they will find in the industry once they graduate, so that they will already know them physically during their academic preparation. So, the Robot was designed and implemented, the mathematical modeling was also obtained, using the RoboAnalyzer software, thus validating results that were normally obtained from the homogeneous transformation matrices of the kinematics and dynamics of the robot movements, to something tangible, such as programming with cards like the PIC microcontroller, Arduino and Raspberry Pi Pico and also manipulate the robot, even with applications with the cell phone,

References

1.   Enrique Ruiz-Velasco Sánchez & Josefina Bárcenas López. (2019). Edutecnología y Aprendizaje 4.0. Instituto de Ciencias Aplicadas y Tecnologías (ICAT), SOMECE. ISBN: 978-607-95656-4-0.

2.   González, Juliana, Carlos Pereyra y Gabriel Vargas (comps.) (1986), Praxis y filosofía. Ensayos en homenaje a Adolfo Sánchez Vázquez. México: Grijalbo.

3.   Andreas Hölldorfer. (2016). Manual de usuario. BCN3D Technologies en colaboración con el Departament d'Ensenyament de la Generalitat de Catalunya.

4.   L.I Yajaira Guadalupe Lázaro Arvizu1, Dr. Roberto Morales Caporal, et. al. (2016). Herramienta Computacional para Manipular un Robot (KUKA) IRB2600 Basada en un Toolbox de MATLAB®/ SIMULINK®. Memorias del congreso internacional de investigación academica Journals 4th, 7.

5. R. Morales Caporal, et. al. (2021). Simplified Reactive Power Control of a Multilevel Inverter for Grid-Connected Photovoltaic Applications, 18th International Conference on Electrical Engineering.

6. GUTIÉRREZ, Cithalih, GONZÁLEZ, Julio y MEZA, José. (2017). Diseño y simulación de un brazo de robot con músculos artificiales de McKibben utilizando CAD. Revista de Ingeniería Mecánica, 1-9, 9.

7. Vinod Kumar, Amit Talli.. (2020). Design, simulation, and analysis of a 6-axis robot using robot visualization software. Conference Series Materials Science and Engineering ·, 5th, 11.

8. O. Michel, Webots: professional mobile robot simulation, Int J.Adv. Robot. Syst.,1(2004), 39–42.

9. Othayoth, R. (2017). Robot kinematics made easy using RoboAnalyzer software. Wiley, (10), p.1.

10. Sasanka Sekhar Sinha. (2018). Inverse Kinematics for General 6R Manipulators in RoboAnalyzer. Joint International Conference on Multibody System Dynamics, 5th, 9.

11. Shailendra Singh Chauhan, Avadhesh Kumar Khare.. (2020). Kinematic Analysis of the ABB IRB 1520 Industrial Robot Using RoboAnalyzer Software. EVERGREEN Joint Journal of Novel Carbon Resource Sciences & Green Asia Strategy, 07, 10.

12. Ramirez Arias, J. (2012). ModelaMiento MateMático de la cinemática directa e inversa de un robot Manipulador de tres grados de libertad. Ingeniería Solidaria, (8), p.7.

[Title in Times New Roman and Bold No. 14 in English and Spanish]

Surname (IN UPPERCASE), Name 1st Author†*, Surname (IN UPPERCASE), Name 1st Coauthor, Surname (IN UPPERCASE), Name 2nd Coauthor and Surname (IN UPPERCASE), Name 3rd Coauthor

Institutional Affiliation of Author including Dependency (No.10 Times New Roman and Italic)

International Identification of Science - Technology and Innovation

ID 1st Author: (ORC ID - Researcher ID Thomson, arXiv Author ID - PubMed Author ID - Open ID) and CVU 1st author: (Scholar-PNPC or SNI-CONACYT) (No.10 Times New Roman)

ID 1st Coauthor: (ORC ID - Researcher ID Thomson, arXiv Author ID - PubMed Author ID - Open ID) and CVU 1st coauthor: (Scholar or SNI) (No.10 Times New Roman)

ID 2nd Coauthor: (ORC ID - Researcher ID Thomson, arXiv Author ID - PubMed Author ID - Open ID) and CVU 2nd coauthor: (Scholar or SNI) (No.10 Times New Roman)

ID 3rd Coauthor: (ORC ID - Researcher ID Thomson, arXiv Author ID - PubMed Author ID - Open ID) and CVU 3rd coauthor: (Scholar or SNI) (No.10 Times New Roman)

Abstract (In English, 150-200 words)

Objectives
Methodology
Contribution

Keywords (In English)

Indicate 3 keywords in Times New Roman and Bold No. 10

Abstract (In Spanish, 150-200 words)

Objectives
Methodology
Contribution

Keywords (In Spanish)

Indicate 3 keywords in Times New Roman and Bold No. 10

Citation: Surname (IN UPPERCASE), Name 1st Author, Surname (IN UPPERCASE), Name 1st Coauthor, Surname (IN UPPERCASE), Name 2nd Coauthor and Surname (IN UPPERCASE), Name 3rd Coauthor. Paper Title. ECORFAN Journal-Democratic Republic of Congo. Year 1-1: 1-11 [Times New Roman No.10]

---

* Correspondence to Author (example@example.org)
† Researcher contributing as first author.

Instructions for Scientific, Technological and Innovation Publication

Introduction

Text in Times New Roman No.12, single space.

General explanation of the subject and explain why it is important.

What is your added value with respect to other techniques?

Clearly focus each of its features

Clearly explain the problem to be solved and the central hypothesis.

Explanation of sections Article.

## Development of headings and subheadings of the article with subsequent numbers

[Title No.12 in Times New Roman, single spaced and bold]

Products in development No.12 Times New Roman, single spaced.

## Including graphs, figures and tables-Editable

In the article content any graphic, table and figure should be editable formats that can change size, type and number of letter, for the purposes of edition, these must be high quality, not pixelated and should be noticeable even reducing image scale.

[Indicating the title at the bottom with No.10 and Times New Roman Bold]
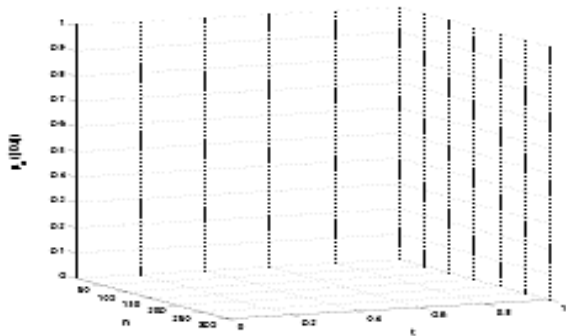
Graphic 1 Title and *Source (in italics)*

Should not be images-everything must be editable.
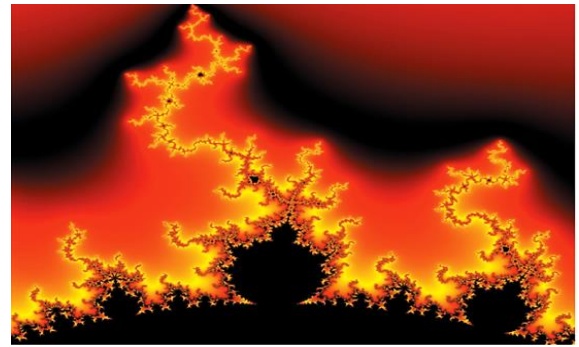
Figure 1 Title and *Source (in italics)*

Should not be images-everything must be editable.

Table 1 Title and *Source (in italics)*

Should not be images-everything must be editable.

Each article shall present separately in **3 folders**: a) Figures, b) Charts and c) Tables in .JPG format, indicating the number and sequential Bold Title.

For the use of equations, noted as follows:

$$Y_{ij} = \alpha + \sum_{h=1}^{r} \beta_h X_{hij} + u_j + e_{ij} \qquad (1)$$

Must be editable and number aligned on the right side.

Methodology

Develop give the meaning of the variables in linear writing and important is the comparison of the used criteria.

Results

The results shall be by section of the article.

Annexes

Tables and adequate sources

Thanks

Indicate if they were financed by any institution, University or company.

Conclusions

Explain clearly the results and possibilities of improvement.

Surname (IN UPPERCASE), Name 1st Author, Surname (IN UPPERCASE), Name 1st Coauthor, Surname (IN UPPERCASE), Name 2nd Coauthor and Surname (IN UPPERCASE), Name 3rd Coauthor. Paper Title ECORFAN Journal-Democratic Republic of Congo. Year [Times New Roman No. 8]

References

Use APA system. Should not be numbered, nor with bullets, however if necessary numbering will be because reference or mention is made somewhere in the Article.

Use Roman Alphabet, all references you have used must be in the Roman Alphabet, even if you have quoted an Article, book in any of the official languages of the United Nations (English, French, German, Chinese, Russian, Portuguese, Italian, Spanish, Arabic), you must write the reference in Roman script and not in any of the official languages.

Technical Specifications

Each article must submit your dates into a Word document (.docx):

Journal Name
Article title
Abstract
Keywords
Article sections, for example:

1. *Introduction*
2. *Description of the method*
3. *Analysis from the regression demand curve*
4. *Results*
5. *Thanks*
6. *Conclusions*
7. *References*

Author Name (s)
Email Correspondence to Author
References

Intellectual Property Requirements for editing:

- Authentic Signature in Color of <u>Originality Format</u> Author and Coauthors.

- Authentic Signature in Color of the <u>Acceptance Format</u> of Author and Coauthors.

- Authentic Signature in blue colour of the <u>Conflict of Interest Format</u> of Author and Co-authors

Reservation to Editorial Policy

ECORFAN-Democratic Republic of Congo reserves the right to make editorial changes required to adapt the Articles to the Editorial Policy of the Journal. Once the Article is accepted in its final version, the Journal will send the author the proofs for review. ECORFAN® will only accept the correction of errata and errors or omissions arising from the editing process of the Journal, reserving in full the copyrights and content dissemination. No deletions, substitutions or additions that alter the formation of the Article will be accepted.

Code of Ethics - Good Practices and Declaration of Solution to Editorial Conflicts

Declaration of Originality and unpublished character of the Article, of Authors, on the obtaining of data and interpretation of results, Acknowledgments, Conflict of interests, Assignment of rights and Distribution

The ECORFAN-Mexico, S.C Management claims to Authors of Articles that its content must be original, unpublished and of Scientific, Technological and Innovation content to be submitted for evaluation.

The Authors signing the Article must be the same that have contributed to its conception, realization and development, as well as obtaining the data, interpreting the results, drafting and reviewing it. The Corresponding Author of the proposed Article will request the form that follows.

Article title:

–   The sending of an Article to ECORFAN-Democratic Republic of Congo emanates the commitment of the author not to submit it simultaneously to the consideration of other series publications for it must complement the Format of Originality for its Article, unless it is rejected by the Arbitration Committee, it may be withdrawn.

–   None of the data presented in this article has been plagiarized or invented. The original data are clearly distinguished from those already published. And it is known of the test in PLAGSCAN if a level of plagiarism is detected Positive will not proceed to arbitrate.

–   References are cited on which the information contained in the Article is based, as well as theories and data from other previously published Articles.

–   The authors sign the Format of Authorization for their Article to be disseminated by means that ECORFAN-Mexico, S.C. In its Holding Democratic Republic of Congo considers pertinent for disclosure and diffusion of its Article its Rights of Work.

–   Consent has been obtained from those who have contributed unpublished data obtained through verbal or written communication, and such communication and Authorship are adequately identified.

–   The Author and Co-Authors who sign this work have participated in its planning, design and execution, as well as in the interpretation of the results. They also critically reviewed the paper, approved its final version and agreed with its publication.

–   No signature responsible for the work has been omitted and the criteria of Scientific Authorization are satisfied.

–   The results of this Article have been interpreted objectively. Any results contrary to the point of view of those who sign are exposed and discussed in the Article.

Copyright and Access

Article Title:

Name and Surnames of the Contact Author and the Coauthors	Signature
1.	
2.	
3.	
4.	

Principles of Ethics and Declaration of Solution to Editorial Conflicts

Editor Responsibilities

The Publisher undertakes to guarantee the confidentiality of the evaluation process, it may not disclose to the Arbitrators the identity of the Authors, nor may it reveal the identity of the Arbitrators at any time.

The Editor assumes the responsibility to properly inform the Author of the stage of the editorial process in which the text is sent, as well as the resolutions of Double-Blind Review.

The Editor should evaluate manuscripts and their intellectual content without distinction of race, gender, sexual orientation, religious beliefs, ethnicity, nationality, or the political philosophy of the Authors.

The Editor and his editing team of ECORFAN® Holdings will not disclose any information about Articles submitted to anyone other than the corresponding Author.

The Editor should make fair and impartial decisions and ensure a fair Double-Blind Review.

Responsibilities of the Editorial Board

The description of the peer review processes is made known by the Editorial Board in order that the Authors know what the evaluation criteria are and will always be willing to justify any controversy in the evaluation process. In case of Plagiarism Detection to the Article the Committee notifies the Authors for Violation to the Right of Scientific, Technological and Innovation Authorization.

Responsibilities of the Arbitration Committee

The Arbitrators undertake to notify about any unethical conduct by the Authors and to indicate all the information that may be reason to reject the publication of the Articles. In addition, they must undertake to keep confidential information related to the Articles they evaluate.

Any manuscript received for your arbitration must be treated as confidential, should not be displayed or discussed with other experts, except with the permission of the Editor.

The Arbitrators must be conducted objectively, any personal criticism of the Author is inappropriate.

The Arbitrators must express their points of view with clarity and with valid arguments that contribute to the Scientific, Technological and Innovation of the Author.

The Arbitrators should not evaluate manuscripts in which they have conflicts of interest and have been notified to the Editor before submitting the Article for Double-Blind Review.

Responsibilities of the Authors

Authors must guarantee that their articles are the product of their original work and that the data has been obtained ethically.

Authors must ensure that they have not been previously published or that they are not considered in another serial publication.

Authors must strictly follow the rules for the publication of Defined Articles by the Editorial Board.

The authors have requested that the text in all its forms be an unethical editorial behavior and is unacceptable, consequently, any manuscript that incurs in plagiarism is eliminated and not considered for publication.

Authors should cite publications that have been influential in the nature of the Article submitted to arbitration.

Information services

Indexation - Bases and Repositories

RESEARCH GATE (Germany)
GOOGLE SCHOLAR (Citation indices-Google)
REDIB (Ibero-American Network of Innovation and Scientific Knowledge- CSIC)
MENDELEY (Bibliographic References Manager)

Publishing Services

Citation and Index Identification H
Management of Originality Format and Authorization
Testing Article with PLAGSCAN
Article Evaluation
Certificate of Double-Blind Review
Article Edition
Web layout
Indexing and Repository
ArticleTranslation
Article Publication
Certificate of Article
Service Billing

Editorial Policy and Management

31 Kinshasa 6593 – Republique Démocratique du Congo. Phones: +52 1 55 6159 2296, +52 1 55 1260 0355, +52 1 55 6034 9181; Email: contact@ecorfan.org www.ecorfan.org

ECORFAN Journal-Democratic Republic of Congo

"Development of an artificial neural network for the prediction of the thermodynamic property enthalpy in the NH_3-H_2O mixture"
VERA-ROMERO, Iván, PEREZ-AVIÑA, L. Fernando, MÉNDEZ-ÁBREGO, V. Manuel and MARTÍNEZ-REYES, José
Universidad de la Ciénega del Estado de Michoacán de Ocampo

"Rotor crack moment of inertia"
JIMÉNEZ RABIELA, Homero, VÁZQUEZ GONZÁLEZ, Benjamín, RAMÍREZ CRUZ, José Luis e ILIZALITURRI BADILLO, Joshua Suraj
Universidad Autónoma Metropolitana

"Analysis of the use of aerogel as a thermal insulator in refrigerated containers for storing blood using a photovoltaic system"
VALLE-HERNANDEZ, Julio, MANZANO-MUÑOZ, Meily Yoselin, ROMÁN-AGUILAR, Raúl and DELGADILLO-AVILA, Wendy Montserrath
Universidad Autónoma del Estado de Hidalgo

"Design and 3D printing of the Robot, articulated with 6 degrees of freedom with educational applications"
SÁNCHEZ-GUARNEROS, Raziel, MARTÍNEZ-HERNÁNDEZ, Haydee Patricia, CORTES-MALDONADO, Raúl and BEDOLLA-HERNÁNDEZ, Jorge
Instituto Tecnológico de Apizaco